Published in final edited form as:
J Comp Neurol. 2009 February 10; 512(5): 664–687. doi:10.1002/cne.21912.

Tracer Coupling Patterns of the Ganglion Cell Subtypes in the Mouse Retina

BÉLA VÖLGYI[1,*], **SAMIR CHHEDA**[1], and **STEWART A. BLOOMFIELD**[1,2]

[1]Department of Ophthalmology, New York University School of Medicine, New York, New York 10016

[2]Department of Physiology & Neuroscience, New York University School of Medicine, New York, New York 10016

Abstract

It is now clear that electrical coupling via gap junctions isprevalent across the retina, expressed by each of the fivemain neuronal types. With the introduction of mutants inwhich selective gap junction connexins are deleted, themouse has recently become an important model for studyingthe function of coupling between retinal neurons. In thisstudy we examined the tracer-coupling pattern of ganglioncells by injecting them with the gap junction-permanenttracer Neurobiotin to provide, for the first time, a comprehensivesurvey of ganglion cell coupling in the wildtypemouse retina. Murine ganglion cells were differentiated into22 morphologically distinct subtypes based on somadendriticparameters. Most (16/22) ganglion cell subtypes were tracer-coupled to neighboring ganglion and/or amacrinecells. The amacrine cells coupled to ganglion cellsdisplayed either polyaxonal or wide-field morphologies withextensive arbors. We found that different subtypes of ganglioncells were never coupled to one another, indicatingthat they subserved independent electrical networks. Finally, we found that the tracer-coupling patterns of the 22ganglion cell populations were largely stereotypic acrossthe 71 retinas studied. Our results indicate that electricalcoupling is extensive in the inner retina of the mouse, suggestingthat gap junctions play essential roles in visual information processing.

Keywords

tracer-coupling; gap junction; ganglion cell; amacrine cell; mouse

With the discovery of gap junction-permeant biotinylated tracers and the constituent connexin proteins, there is now mounting evidence that electrical synaptic transmission via gap junctions forms a prevalent mode of intercellular communication in the central nervous system (CNS; reviewed by Meier and Dermietzel, 2006). An elegant example is the vertebrate retina, in which each of the five major neuronal types is coupled via gap junctions. In many instances the coupling strength is dynamically regulated by ambient illumination acting through light-activated neuromodulators such as dopa-mine and nitric oxide (Mills and Massey, 1995; Bloomfield et al., 1997; Baldridge et al., 1998; Xin and Bloomfield, 1999, 2000; Weiler et al., 2000; He et al., 2000). The networks formed by electrically coupled neurons thus provide plastic, reconfigurable circuits positioned to play key and diverse roles in the transmission and processing of visual information at every retinal level.

[*]Correspondence to: Dept. Ophthalmology, NYU School of Medicine, 550 First Ave., New York, NY 10016. volgyb01@med.nyu.edu.

The variety of gap junctional connections is the richest in the proximal retina, in which homologous and heterologous coupling occurs between dendrites of ganglion and amacrine cells and the axon terminals of bipolar cells. In fact, it appears that most of the ≈50 subtypes of amacrine and ganglion cells in the mammalian retina are electrically coupled (Vaney, 1991; Xin and Bloomfield, 1997). This complex organization suggests that gap junctions play a variety of roles in integrating visual signals just as they leave the retina for higher brain structures. Although the function of only a few of these gap junctions have been studied, they indeed appear to play a number of diverse roles, including synchronization of neighboring cell activity, increasing response signal-to-noise, and mixing of rod- and cone-mediated signals (Mastronarde, 1983a–c; Brivanlou et al., 1998; DeVries, 1999; Feigenspan et al., 2001; Deans et al., 2002; Bloomfield and Völgyi, 2004; Maxeiner et al., 2005).

To fully understand the functional roles played by different gap junctions, it is first necessary to elucidate the organization of the electrical synaptic circuitry by determining the coupling patterns of specific amacrine and ganglion cell subtypes. It is particularly important to determine the electrical circuitry in the mouse retina, as mutant reporter and connexin knockout models have become important subjects for determining the distribution and function of gap junctions in the retina (Güldenagel et al., 2001; Deans et al., 2002; Hombach et al., 2004; Völgyi et al., 2004; Maxeiner et al., 2005; Shelley et al., 2006).

In the present study we examined the coupling pattern of the different ganglion cell subtypes in the dark-adapted mouse retina by injecting them with the gap junction-permeant tracer Neurobiotin. We differentiated 22 morphologically distinct ganglion cell populations, most of which corresponded to subtypes characterized previously in the mouse retina (Sun et al., 2002; Badea and Nathans, 2004; Kong et al., 2005; Coombs et al., 2006). We found that murine ganglion cells show a wide variety of coupling patterns, including heterologous coupling to neighboring wide-field and polyaxonal amacrine cells and/or homologous coupling between nearby ganglion cells. Interestingly, no evidence for coupling between different ganglion cell subtypes was found, suggesting that they subserve separate electrical circuits. Moreover, we found that most of the distinct ganglion cell subtypes in the mouse retina maintained a stereotypic coupling pattern indicating that they subserve discrete electrical networks.

MATERIALS AND METHODS

Preparation

Adult ($P_{30–90}$) C57BL6 wildtype (WT) mice were deeply anesthetized with an intraperitoneal injection of Nembutal (0.08 g/g bodyweight) and lidocaine hydrochloride (20 mg/mL) applied locally to the eyelids and surrounding tissue. A flattened retinal-scleral preparation developed for rabbit (Hu et al., 2000) was adopted and modified for the mouse. Briefly, the eye was removed under dim red illumination and hemisected anterior to the ora-serrata. Anterior optics and the vitreous humor were removed and the resultant retina-eyecup was placed in a superfusion chamber. Several radial incisions were made peripherally allowing the eyecup to be flattened. The chamber was then mounted in a light-tight Faraday cage and superfused with an oxygenated mammalian Ringer solution (pH = 7.4, 32°C; Bloomfield and Miller, 1982). Retinas were dark-adapted for 1 hour prior to experimentation. Animals were sacrificed immediately after enucleations. All animal procedures were in compliance with the NIH Guide for the Care and Use of Laboratory Animals and approved by the Institutional Animal Care and Use Committee at NYU School of Medicine.

Neurobiotin injections

Ganglion cells were visualized using trans-scleral illumination with infrared (IR) light and impaled with standard boro-silicate glass microelectrodes (Sutter Instrument, Novato, CA). The use of IR light allowed us to visualize cells while maintaining retinas in a dark-adapted state. Electrodes were filled at their tips with 4% N-(2-amino-ethyl)-biotinamide hydrochloride (Neurobiotin, Vector Laboratories, Burlingame, CA), in 0.1 M Tris buffer (pH = 7.6) and then backfilled with 4 M potassium chloride. Relatively large (>10 μm in diameter) cell bodies were targeted with glass electrodes at random retinal locations to try and sample across the entire population of ganglion cell subtypes. Neurobiotin was iontophoresed into impaled neurons using a sinusoidal (3 Hz, 0.8 nA peak-to-peak) current for 15 minutes. Since there was an inherent bias toward larger somata as to the success of electrode impalement, we have not attempted to correlate the relative number of each ganglion cell subtype in our sample with their distribution frequency in the retina.

Histology

One hour after labeling the last cell in an experiment, the retina was fixed overnight in a cold (4°C) solution of 4% paraformaldehyde in 0.1 M phosphate buffer (PB; pH = 7.3). Retinas were then washed in PB and soaked in a solution of 0.18% hydrogen peroxide in methyl alcohol for 1 hour. This treatment completely abolished the endogenous peroxidase activity. Retinas were then washed in PB and reacted with the Elite ABC kit (Vector Laboratories) and 1% Triton X-100 in sodium phosphate-buffered saline (PBS; 9% saline, pH = 7.6). Retinas were subsequently processed for peroxidase histo-chemistry using 3,3′-diaminobenzidine (DAB), dehydrated, and flat-mounted for light microscopy.

Digital images of labeled neurons were captured by a cooled CCD camera (Spot 2, Diagnostic Instruments, Sterling Heights, MI) followed by software manipulation of brightness and contrast (Photoshop, Adobe Systems, San Jose, CA). Drawings of cells were made using a camera-lucida microscope attachment and then digitized by scanner. To determine the level at which dendritic processes stratified in the inner plexiform layer (IPL), we examined Neurobiotin-labeled cells in flat mount under a 100× oil-immersion lens. The borders of the IPL were determined by the location at which amacrine and ganglion cell bodies were defocused using Nomarski interference contrast optics. The position of the outer margin of the IPL next to the amacrine cell bodies was defined as 0% depth, whereas the vitreal border of the IPL next to the ganglion cell bodies was defined as 100% depth. The position of cellular processes in the IPL was determined using a precision micrometer and given a depth value of 0–100%. Multiple measures were made for a single cell to reveal any variations in stratification throughout the extent of its arbor.

RESULTS

A total of 210 retinal ganglion cells were injected with Neurobiotin in 71 WT mice to determine their tracer-coupling patterns. Previous studies have found no observable relationship between ganglion cell dendritic field or soma sizes and retinal eccentricities in the mouse (Jeon et al., 1998; Sun et al., 2002). This unique feature of the mouse retina allowed us to collect data for each ganglion cell population through injections made at various retinal eccentricities. To identify each injected ganglion cell, we carried out a thorough morphometric analysis of several parameters, including: 1) shape of soma; 2) soma size; 3) dendritic field diameter; 4) dendritic morphology, including the existence or lack of dendritic specializations (e.g., swellings, spines); 5) dendritic branching pattern, and; 6) stratification levels of dendrites in the IPL. Based on these criteria, we differentiated 22 ganglion cell populations (see Table 1, Fig. 13), which were then correlated with ganglion cell subtypes described previously using either a similar morphometric (Sun et al., 2002) or

cluster analyses (Badea and Nathans, 2004; Kong et al., 2005; Coombs et al., 2006). Results of this comparison are summarized in Table 2. We found that morphologies of the most common ganglion cell groups in this study were very similar to the 17 ganglion cell subtypes characterized by Sun et al. (2002). Due to this strong correlation, we chose not to create a new characterization scheme, but to rather use the nondescriptive terminology of G_1 to G_{17} to name these 17 ganglion cell subtypes. In addition, we include in this study five ganglion cells (G_{18} to G_{22}) that were rarely encountered. Although these five cells appear to have no counterparts in the Sun et al. (2002) study, four of them (G_{18},G_{20},G_{21}, and G_{22}) have been described previously by others (Badea and Nathans, 2004; Kong et al., 2005; Coombs et al., 2006).

Ganglion cell subtypes

G_1 ganglion cells (n = 8)—G_1 cells in the mouse retina displayed large (21 μm diameter), polygonal somata and one of the largest dendritic arbors (245 μm diameter) in our sample. Three to five short primary dendrites branched up to five times and stratified in sublamina-b at an IPL depth of 78% (Figs. 1A,B, 13). Even the highest-order branch points were relatively close to the soma, thus resulting in long terminal dendrites that sometimes overlapped. Based on these morphological features, our G_1 cells appear homologous with the giant cells described in the rat retina (Bunt et al., 1976; Huxlin and Goodchild, 1997). Moreover, they show strong homology with mouse ganglion cells described in previous studies, including A1 cells (Sun et al., 2002), cells in monostratified cluster 9 (Badea and Nathans, 2004), cluster 11 (Kong et al., 2005), and cells in cluster M10 (Coombs et al., 2006).

G_1 ganglion cells showed heterologous tracer coupling to up to 17 amacrine cells with relatively large cell bodies (≈12 μm in diameter) and up to 21 other amacrine cells with somewhat smaller somata (≈8 μm in diameter) (Fig. 1A,B), which were displaced to the ganglion cell layer. It is important to note that here and for the other ganglion cell subtypes described below, we often found tracer coupling to amacrine cells with different sized somata. We believe that this reflects coupling to multiple subtypes of amacrine cells. Since we often could not visualize their dendritic morphologies, this categorization of amacrine cells remains speculative. However, we were able to visualize the detailed morphology of the amacrine cells that were coupled to G_1 ganglion cells. Both populations of tracer-coupled amacrine cells displayed relatively thick and short dendrites as well as thin and long axon-like processes (Fig. 1B–D), identifying them as polyaxonal amacrine cells (Famiglietti, 1992a,b; Stafford and Dacey, 1997; Völgyi et al., 2001). Both dendrites and axons costratified with G_1 ganglion cell dendrites at IPL depths of 72% and 69%, respectively.

During the course of this study we occasionally injected the somata of amacrine cells displaced to the GCL and were able to visualize their complete morphology. On two occasions we labeled amacrine cells that appeared, based on morphological similarities, to be the large amacrine cell that is coupled to G_1 cells. These similarities included soma shape and size (≈14 μm in diameter), displaced location of cell bodies, size of the dendritic arbor (≈200 μm in diameter), and stratification level of dendrites (73%) and axonal (71%) processes in the IPL (Fig. 2A,B). These well-stained large amacrine cells displayed axonal processes identifying them as polyaxonal cells. They were tracer coupled to six other amacrine cells with similar soma shape and size (Fig. 2A,C) and to up to five ganglion cells with large (≈19 μm diameter) cell bodies and short primary dendrites similar those displayed by G_1 cells. These large, polyaxonal amacrine cells resemble WA4-1 amacrine cells (Lin and Masland, 2006) and PA-S5 amacrine cells (Pérez De Sevilla Müller et al., 2007) described previously in the mouse retina.

G_2 ganglion cells (n = 19)—The G_2 subtype of ganglion cell showed a number of morphological features similar to those described for ON alpha cells in various mammalian species, including the mouse (Boycott and Wässle, 1974; Peichl et al., 1987a,b; Schubert et al., 2005a; Völgyi et al., 2005a,b). These similarities included a spherical soma (≈18 μm diameter) and stout, smooth dendrites that characteristically branched at acute angles with almost no overlap (Figs. 3A, 13). G_2 cells displayed large symmetrical dendritic arbors (≈200 μm diameter), which unistratified within sublamina-b of the IPL at a 73% depth. Recent morphological studies have described ganglion cells in the mouse retina with very similar soma/ dendritic morphologies, including $A2_i$ cells (Sun et al., 2002), cells in monostratified cluster 9 (Badea and Nathans, 2004), cluster 8 (Kong et al., 2005), and M8 and M9 (on) (Coombs et al., 2006).

G_2 ganglion cells were typically tracer coupled to up to 14 amacrine cells whose somata were displaced to the GCL (Fig. 3A,B). One population of amacrine cells had small, round somata (≈7 μm diameter), whereas the cell bodies of a second population were typically darker and larger (≈10 μm diameter). These larger tracer-coupled amacrine cells displayed 2– 4 primary dendrites that bifurcated at right or obtuse angles within a relatively close distance to the soma (<100 μm) and showed no further branching. The dendrites of some well-labeled, large amacrine cells could be followed for several hundred microns before fading from view (Fig. 3B). Despite their relatively extended length, the processes of these large amacrine cells appeared to form a uniform arbor with no evidence of separate dendritic and axonal systems. The dendrites of the coupled amacrine cells costratified (72% depth of the IPL) with the dendrites of the injected G_2 ganglion cells. Overall, the initial morphology of these tracer-coupled, large amacrine cells is similar to that of the giant amacrine cells in mouse described by Badea and Nathans (2004).

G_3 ganglion cells (n = 58)—G_3 ganglion cells displayed soma/dendritic morphologies characteristic of the OFF alpha cells described in various mammalian species, including the mouse (Boycott and Wässle, 1974; Peichl et al., 1987a,b; Hidaka et al., 2004; Schubert et al., 2005a; Völgyi et al., 2005a,b). These features included: 1) relatively large (≈18 μm diameter) and spherical somata; 2) stout and generally smooth primary dendrites (although the higher order dendrites showed varicosities); 3) stratification of dendrites in sublamina-a at 33% depth of the IPL and; 4) dense and relatively large dendritic arbors (≈185 μm diameter) (Figs. 3C,D, 13). G_3 cells clearly corresponded to the $A2_o$ cells (Sun et al., 2002) and they also shared morphological features with cells in monostratified cluster 7 (Badea and Nathans, 2004), cluster 10 (Kong et al., 2005), and M9(off) (Coombs et al., 2006).

G_3 ganglion cells showed homologous coupling to a group of 3– 8 well-labeled G_3 ganglion cell neighbors (Fig. 3C) and heterologous coupling to two subpopulations of amacrine cells with somata lying within the proximal border of the INL (Fig. 3E). One amacrine cell subtype displayed relatively small, round cell bodies (≈7 μm diameter), whereas the somata of the other subtype were typically larger and spherical (≈10 μm diameter). These latter coupled amacrine cells showed two or three primary dendrites that branched proximally 1–2 times and continued with no further branching. This proximal branching resulted in long terminal dendrites running several hundred microns before termination; these dendrites largely costratified with dendrites of G_3 ganglion cells (Fig. 3D,F). These morphological features resembled those for amacrine cells described as wide-field cluster 3 cells by Badea and Nathans (2004) as well as WA2-2 cells described by Lin and Masland (2006).

G_4 ganglion cells (n = 5)—G_4 ganglion cells had small somata (≈13 μm diameter) and curvy, radial running dendrites (Figs. 4A, 13). Dendrites branched four to six times to form a relatively small arbor (143 μm average diameter). Interestingly, some terminal dendrites were 2–3 times longer than others and stood out from the denser proximal portion of the

arbor. Both short and long terminal dendrites stratified in the middle of the IPL at 46% depth. The morphology of G_4 cells resembled B1 cells (Sun et al., 2002), cells in cluster 2 (Kong et al., 2005), and, to some extent, the cells in monostratified cluster 1 (Badea and Nathans) and M3(off) (Coombs et al., 2006) in the mouse retina.

G_4 ganglion cells showed heterologous tracer-coupling to as many as 30 amacrine cells with relatively small somata (≈7 μm) that lay in the INL (Fig. 4B). Unfortunately, the dendrites of these coupled amacrine cells were insufficiently labeled for further morphological analysis. Thus, it was not clear if these tracer-coupled amacrine cells included one or more subtypes.

G_5 ganglion cells (n = 12)—G_5 ganglion cells had small somata (≈11 μm diameter) and small, but dense dendritic fields (≈105 μm diameter). Dendrites followed a tortuous course and displayed many tiny branches and swellings and stratified somewhat diffusely in the middle of the IPL (50% depth) (Figs. 4C, 13). The soma/dendritic architecture of G_5 cells resembled B2 cells (Sun et al., 2002), cells in monostratified cluster 2 and 4 (Badea and Nathans, 2004), cluster 1 (Kong et al., 2005), and M11 (Coombs et al., 2006) in the mouse retina. G_5 ganglion cells showed no evidence of tracer coupling.

G_6 ganglion cells (n = 19)—The G_6 ganglion cells shared many morphological features with the inner delta ganglion cells described in the rat (Peichl, 1989). These included: 1) a round or elliptical soma (≈19 μm average diameter) (Fig. 4D); 2) radiate primary dendrites that branched at acute angles; and 3) higher-order dendrites that displayed numerous swellings and occasional overlapping (Fig. 4E,F,H). In addition, the dendrites of G_6 ganglion cells stratified narrowly at the 70% depth of the IPL and formed a large dendritic arbor (≈190 μm diameter). We found that some G_6 cells showed a strongly elliptical soma, elongated dendritic field, and wavy dendrites (Figs. 4I, 13). However, all other features of these elongated G_6 cells were similar to those displayed by the other G_6 cells. Both the architecture and stratification of G_6 cell dendrites were identical to those of $B3_i$ cells (Sun et al., 2002), cells in monostratified cluster 9 (Badea and Nathans, 2004), cluster 4 (Kong et al., 2005), and M7(on) and M3(on) (Coombs et al., 2006).

G_6 ganglion cells showed heterologous tracer-coupling to amacrine cells with somata displaced to the GCL. Coupled amacrine cells displayed a variety of soma sizes, suggesting that they comprised more than one subtype (Fig. 4D,F). One group displayed large (≈11 μm diameter) elliptical cell bodies and both dendritic and axonal processes characteristic of polyaxonal amacrine cells (Fig. 4E–J). Both axons and dendrites costratified with dendrites of injected G_6 ganglion cells at a depth of 73% of the IPL. The amacrine cell dendrites tapered gradually and occasionally displayed short side-branches or spines, whereas axons were much thinner, running hundreds of microns in the IPL with no evidence of tapering, but showing many swellings (Fig. 4F–J). Typically, the axons emerged directly from dendritic tips and followed the course of the parent dendrite (Fig. 4G). These coupled polyaxonal cells closely resembled WA4-1 amacrine cells (Lin and Masland, 2006) and PA-S5 amacrine cells (Pérez De Sevilla Müller et al., 2007) in the mouse retina. In addition to these polyaxonal amacrine cells, G_6 ganglion cells were also weakly coupled to as many as 28 small (≈7 μm diameter) amacrine cell somata. Unfortunately, the dendritic arbors of these small, coupled amacrine cells were not visible, making identification of these cells impossible.

G_7 ganglion cells (n = 11)—G_7 ganglion cells shared many morphological features with outer delta ganglion cells described in the rat retina (Peichl, 1989), including a round soma (≈19 μm diameter) and 3–5 thick primary dendrites. Dendrites branched 3– 4 times and stratified at the 30% depth of the IPL (Figs. 5A,B, 13). The dendrites largely ran in radial

directions, but they followed a characteristic meandering course and sometimes wandered vertically between strata. Higher-order dendrites were decorated with swellings and included long terminal branches, resulting in a relatively large arbor (≈196 μm in diameter). The morphology of G_7 cells was identical to $B3_o$ cells (Sun et al., 2002), as well as cells in monostratified cluster 7 (Badea and Nathans, 2004), cluster 6 (Kong et al., 2005), and M6(off) (Coombs et al., 2006).

G_7 ganglion cells showed homologous coupling to an array of neighboring G_7 cells (Fig. 5A). In addition, G_7 ganglion cells showed heterologous coupling to small (≈6 μm diameter) and large (≈10 μm diameter) amacrine cells with cell bodies within the INL (Fig. 5C). This apparent difference between the soma sizes of the amacrine cells indicated that they reflected two distinct subtypes. The soma/dendritic morphology of well-labeled, large coupled cells were examined in detail. Dendrites of these amacrine cells were long (400–500 μm) and straight, followed a radial course, branched only proximally, and stratified at the 37% depth of the IPL. These coupled amacrine cells clearly showed characteristics of wide-field amacrine cells (Fig. 5D) and resembled cells in wide-field cluster 3 (Badea and Nathans, 2004) and WA2-2 amacrine cells (Lin and Masland, 2006).

G_8 ganglion cells (n = 8)—G_8 ganglion cells had mediumsized (≈15 μm diameter), round somata and 6–9 relatively thin and short primary dendrites that branched extensively. Dendritic segments followed a convoluted course, often zigzagging both laterally and/or transversally across several IPL strata. The dendrites had numerous small side-branches, as well as spines and swellings that lent a quite complex appearance to the medium-sized arbor (≈165 μm diameter) (Figs. 5F,H–L, 13). The dendrites of G_8 cells stratified rather broadly between the 45% and 68% depths of the IPL (Fig. 5I–K). The dendritic architecture of G_8 cells resembled B4 cells (Sun et al., 2002), cells in the M1, M11 clusters (Coombs et al., 2006), cells in monostratified cluster 2 and 4 (Badea and Nathans, 2004) and cells in cluster 1 (Kong et al., 2005).

G_8 ganglion cells showed heterologous tracer coupling to amacrine cells with small (≈5 μm diameter) or large (≈10 μm diameter) somata that lay either in the INL or GCL (Fig. 5E,G). This dichotomy of soma sizes suggests that G_8 ganglion cells are coupled to at least two subtypes of amacrine cells. In a few cases the large amacrine cells were well-labeled, allowing for a detailed morphological examination. These amacrine cells had 2–3 primary dendrites that bifurcated once or twice proximally and then ran hundreds of microns without signifi-cant tapering at the 50% depth of the IPL (Fig. 5M). The dendrites of these coupled amacrine cells also displayed some varicosities along their length. These coupled cells resembled the WA3-2 wide-field amacrine cells described by Lin and Masland (2006). However, the limited tracer flow did not allow for the examination of dendritic morphology of small coupled amacrine cells, thus whether the large and small somata of coupled amacrine cells reflect two distinct sub-populations remains speculative.

G_9 ganglion cells (n = 8)—G_9 ganglion cells displayed medium sized (≈14 μm diameter) cell bodies and 3–5 relatively thick primary dendrites (Figs. 6A, 13). Dendrites branched several times often at right angles, were rather straight and displayed swellings on their surface. Dendritic terminals stratified close to the middle of the IPL at 62% depth. The dendritic branches showed almost no overlap and economically tiled the space occupied by the medium-sized dendritic arbor (≈166 μm diameter). G_9 cells corresponded to C1 cells reported by Sun et al. (2002) and resembled cells in monostratified cluster 1 (Badea and Nathans, 2004) and in cluster 2 and 7 (Kong et al., 2005). G_9 ganglion cells showed no evidence of tracer coupling.

G_{10} ganglion cells (n = 8)—G_{10} ganglion cells showed relatively large (≈18 μm diameter) somata and 5– 6 slender primary dendrites. Most primary dendrites of G_{10} ganglion cells ran as long as 25 μm before bifurcating. G_{10} cells maintained sparse arbors that showed up to fourth-order branching often at close to right angles, resulting in little overlap of individual segments (Figs. 6B, 13). While primary and secondary dendrites were relatively straight, terminal dendrites often took a wavy course and even curved back toward the soma before ending. Dendrites stratified mainly at the 71% depth of the IPL, but some dendrites projected proximally to depths of 84–92% adjacent to the GCL. The dendritic arbors of G_{10} ganglion cells were among the largest in our sample (247 μm average diameter). These morphological features of G_{10} cells were identical to $C2_i$ cells (Sun et al., 2002), to cells in monostratified cluster 9 (Badea and Nathans, 2004), to cells in cluster 11 (Kong et al., 2005) and cells in M6(on) and M10 clusters (Coombs et al., 2006).

G_{10} ganglion cells displayed heterologous tracer coupling to up to 20 amacrine cells with cell bodies displaced to the GCL (Fig. 6B,C). These coupled amacrine cells maintained cells bodies with either round (≈7 μm in diameter) or elliptical shape (long axis of ≈12 μm). Both dendritic and axonal processes of the coupled amacrine cells could often be visualized, identifying them as polyaxonal cells. The dendrites and axonal processes of the coupled polyaxonal cells costratified with G_{10} ganglion cell processes at the 72–73% of the IPL. On one occasion, we injected Neurobiotin into a displaced amacrine cell, revealing morphological features that matched those of the polyaxonal cells coupled to G_{10} ganglion cells (Fig. 6D). Dendrites of this polyaxonal amacrine cell appeared stout, wavy, and displayed occasional small side-branches. In contrast, the axons displayed numerous swellings and extended over 1 mm (Fig. 6D,E). This amacrine cell was coupled to other amacrine cells with both round (≈7 μm diameter) and elliptical somata displaced to the GCL (Fig. 6D, left, and F). In addition, this cell was coupled to eight ganglion cells with morphological features similar to those of G_{10} cells, including large somata, bifurcating primary dendrites, stratification level in the IPL (73%), and relatively loose dendritic arbor (Fig. 6D, left, F,G). This polyaxonal amacrine cell shared many morphological features with the WA4-1 amacrine cell type described by Lin and Masland (2006).

G_{11} ganglion cells (n = 12)—G_{11} ganglion cells displayed relatively large somata (≈17 μm diameter) and dendritic arbors (≈183 μm diameter). The dendritic architecture of G_{11} cells showed many similarities to that of G_{10} cells, including 3–5 thin, primary dendrites that branched distally at acute angles with terminal endings that typically curved backwards (Figs. 7A–E, 13). However, in clear contrast to G_{10} cells, the dendrites of G_{11} cells had a wavy appearance throughout and stratified mainly in sublamina-a at the 31% depth of the IPL. Overall, the morphological features of G_{11} cells resembled the $C2_o$ cells of Sun et al. (2002), cells in monostratified cluster 7 of Badea and Nathans (2004) and M6(off) of Coombs et al. (2006).

Interestingly, G_{11} cells showed some variability in their tracer-coupling patterns. Most G_{11} ganglion cells displayed homologous coupling to up to seven ganglion cells (Fig. 7D), clearly identified by the size and the location of their somata and the presence of an axon that entered the optic disk (not shown). In addition, G_{11} cells showed heterologous coupling to amacrine cells with small (≈6 μm diameter) and round somata in the INL (Fig. 7C,E). The dendrites of tracer-coupled amacrine cells were visualized in one injection and found to stratify at 27% depth of the IPL. However, due to the faint labeling of dendrites, further identification of this coupled amacrine cell was not possible. Three G_{11} cells failed to show the homologous coupling to ganglion cells but otherwise shared all their morphological features with the other G_{11} cells (Fig. 7A–C).

G_{12} ganglion cells (n = 3)—G_{12} ganglion cells showed relatively small somata (≈14 μm diameter) and large dendritic arbors (≈200 μm diameter). The arbor consisted of dendrites that branched irregularly, displayed numerous swellings and terminal branches that were very long (Figs. 7F–H, 13). Overall, G_{12} cells displayed a rather sparse and irregular dendritic architecture. G_{12} cells showed bistratification of dendrites at the 33% and 67% depths of the IPL. The morphological features of G_{12} cells resembled somewhat descriptions of C3 cells (Sun et al., 2002), melanopsin expressing cells in cluster M6(on) (Coombs et al., 2006), type 1 cells by Schubert et al. (2005b) and an unnamed bistratified cell in descriptions of Coombs et al. (2006). G_{12} ganglion cells displayed no evidence of tracer coupling (Fig. 7H), analogous to the uncoupled type 1 cells described by Schubert et al. (2005b).

G_{13} ganglion cells (n = 9)—G_{13} ganglion cells displayed medium-sized somata (≈15 μm diameter) and dendritic arbors (≈160 μm diameter) (Figs. 8A–F, 13). They showed 4–7 short, primary dendrites that often branched immediately after emerging from the soma. Dendrites then branched repetitively and displayed swellings, spine-like structures, and short side-branches. Larger dendritic segments zigzagged horizontally and/or vertically between IPL strata. (Fig. 8B–D,F). This zigzagging, in combination with the convoluted branching pattern, gave a rather dense appearance to G_{13} cell dendritic arbors that stratified diffusely between the 39 – 65% depths of the IPL (Fig. 8B–D). The dendritic architecture and stratification of G_{13} cells resembled most cells in monostratified clusters 4 and 5 (Badea and Nathans, 2004), cells in cluster M11 (Coombs et al., 2006), in cluster 1 (Kong et al., 2005), and, less so, the C4 cells of Sun et al. (2002). It should be noted that the G_{13} and G_8 ganglion cells showed strong similarities in terms of their soma size, dendritic field size, and stratification of dendrites. However, these two ganglion cell populations were distinguishable based on the denser dendritic field and finer dendritic processes of G_8 ganglion cells.

G_{13} ganglion cells showed homologous tracer coupling to up to 10 nearby ganglion cells whose shape and size were identical to the injected G_{13} cell somata (Fig. 8A). G_{13} ganglion cells also displayed heterologous coupling to amacrine cells with either small (≈6 μm diameter) or large (≈10 μm diameter) somata found both in the INL and GCL (Fig. 8A,E). Although the coupled amacrine cells were never labeled well enough for clear morphological identification, visualized dendrites stratified close to the middle of the IPL at a 59% depth.

G_{14} ganglion cells (n = 3)—G_{14} ganglion cells displayed relatively small somata (≈13 μm diameter) and dendritic arbors (≈135 μm diameter) (Figs. 9A,B, 13). They typically showed 5–7 thin, primary dendrites that branched proximally, curved extensively, but generally ran in radial directions. Higher-order dendrites displayed numerous swellings and spines. The dendritic arbor of G_{14} cells monostratified narrowly within the middle of the IPL at a 51% depth. G_{14} cells shared many morphological features with monostratified cluster 1–2 cells of Badea and Nathans (2004), cluster 2 cells of Kong et al. (2005), C5 cells of Sun et al. (2002), and M3(off) cells of Coombs et al. (2006). G_{14} ganglion cells showed no evidence of tracer-coupling.

G_{15} ganglion cells (n = 3)—G_{15} ganglion cells had relatively large somata (≈18 μm diameter) and medium-sized dendritic arbors (≈153 μm diameter) (Figs. 9C,D, 13). The dendritic arbor of G_{15} cells showed a characteristic anisotropy with branches confined to one side of the cell body. G_{15} cells displayed 3–5 primary dendrites that often emerged from a single stalk and then branched occasionally in undulating segments that displayed occasional swellings (Fig. 9D). While intermediate dendrites meandered up and down

between IPL strata, most terminal dendrites stratified at the 25% depth of the IPL. The morphology of G_{15} cells was essentially the same as those of C6 cells (Sun et al., 2002), monostratified cluster 6 cells (Badea and Nathans, 2004), M5a cells (Coombs et al., 2006), and JAM-B-positive ganglion cells by Kim et al. (2008).

G_{15} ganglion cells displayed heterologous tracer coupling to amacrine cells with somata that lay in the proximal INL (Fig. 9E). These coupled amacrine cells had medium-sized (6 – 8 μm diameter) somata and appeared to reflect a single sub-type. Unfortunately, the labeling of these coupled amacrine cells was restricted to the somata and so further identification was not possible.

G_{16} ganglion cells (n = 3)—G_{16} ganglion cells had small cell bodies (≈14 μm diameter) and dendritic arbors (≈123 μm diameter) (Figs. 10A–C, 13). The bistratified dendritic arbor (30% and 56% depths) consisted of very fine, tortuous segments that showed up to sixth-order branching. Some of the terminal dendrites were rather long and appeared to project out from the rest of the dendritic arbor. The dendrites in sublamina-a were more wavy and displayed more swellings than those in sublamina-b. G_{16} cells showed overall morphology similar to the D1 cells of Sun et al. (2002), bistratified cluster 1 cells of Badea and Nathans (2004), and type 3 cells of Schubert et al. (2005b).

G_{16} ganglion cells were tracer coupled to 4 – 6 nearby cell bodies in the GCL (Fig. 10A). Some of these coupled cells were clearly identified as ganglion cells based on the presence of an axon. Moreover, the soma size and shape of these coupled ganglion cells suggested that they were also G_{16} cells. G_{16} cells showed no evidence of heterologous coupling to neighboring amacrine cells (Fig. 10A,C). Our results are consistent with those of Schubert et al. (2005b) showing that their type 3 cells maintain homologous, but not heterologous coupling.

G_{17} ganglion cells (n = 16)—G_{17} ganglion cells had medium-sized somata (≈15 μm diameter) and dendritic arbors (≈160 μm diameter) (Figs. 10D–F, 13). G_{17} ganglion cells displayed 3–5 stout primary dendrites that often ran 10–15 μm before branching. Second- and higher-order dendrites were considerably thinner and showed undulations and swellings. The dendritic arbor bistratified at 32% and 68% depths of the IPL. Similar to G_{16} cells, the dendrites of G_{17} cells within sublamina-a of the IPL displayed more undulations and swellings than those in sublamina-b. The morphology of G_{17} cells was very similar to that of D2 cells of Sun et al. (2002) and type 2 cells of Schubert et al. (2005b) in the mouse retina. These cells appear to be the murine homolog of the ON-OFF direction selective ganglion cells described in other mammalian retinas (Vaney, 1991, 1994; Xin and Bloomfield, 1997). G_{17} cells also shared many morphological features with bistratified cluster 2 and 3 of Badea and Nathans (2004) and M12, M13, and M14 cluster cells of Coombs et al. (2006).

G_{17} ganglion cells were coupled to other ganglion cell bodies in the GCL identified by their axons that ran to the optic disk (Fig. 10D). Some well-labeled coupled cells displayed dendritic stratification and morphology identical to those of the injected G_{17} cells. In contrast, G_{17} cells showed no evidence of tracer coupling to neighboring amacrine cells (Fig. 10D,F). Our results are consistent with those of Schubert et al. (2005b) showing that type 2 cells maintain homologous, but not heterologous coupling.

Rarely encountered ganglion cell subtypes

The ganglion cell subtypes in this section were each encountered only once during this study. Whether this reflects their low distribution in the retina or a sampling bias is unclear. However, each subtype showed a unique soma/dendritic morphology that clearly distinguished them from the other ganglion cell subtypes we described.

G_{18} ganglion cell (n = 1)—The G_{18} ganglion cell had a medium-sized soma (≈15 μm diameter) and the smallest dendritic field (62 μm diameter) of all the ganglion cells in our sample (Figs. 11A,E, 13). The G_{18} cell showed three primary dendrites that branched to form an arbor with fourth- to fifth-order branches. Dendrites were tortuous and displayed many swellings (Fig. 11B,C,E,F). The terminal dendrites of the G_{18} ganglion cell stratified narrowly at the 25% depth of the IPL (Fig. 11C). The G_{18} cell shared most morphological features with cells in monostratified cluster 4 (Badea and Nathans, 2004) and cells in cluster 6 (Kong et al., 2005).

The G_{18} cell showed homologous coupling to 11 ganglion cell neighbors. These coupled cells were identified unequivocally as G_{18} cells based on their soma/dendritic morphologies (Fig. 11A,E,F). The coupled ganglion cell somata were relatively close to each other, and their dendritic arbors showed a considerable overlap. The G_{18} cell also showed extensive heterologous coupling to amacrine cells somata that lay either in the GCL or in the IPL (Fig. 11A,D). The similar shape and size (≈7 μm diameter) as well as the even distribution of these coupled amacrine cell somata suggested that they formed a single subtype.

G_{19} ganglion cell (n = 1)—The G_{19} ganglion cell displayed a unique dendritic morphology consisting of only one dendrite that meandered vertically within the IPL (between the 20 – 42% depths) (Figs. 11G,H, 13). The sole dendrite of this cell showed only a few very short side-branches (Fig. 11H). Interestingly, the axon of this ganglion cell also showed some small side-branches before it joined other fibers to enter the optic disk (Fig. 11G,I). This G_{19} cell did not have a counterpart in previous morphological studies and, in fact, we encountered it only once in our study. Thus, the G_{19} cell appears to be rare. The G_{19} ganglion cell showed no evidence of tracer coupling.

G_{20} ganglion cell (n = 1)—The G_{20} cell had a medium-sized cell body (≈14 μm in diameter) and a relatively small dendritic arbor (≈117 μm diameter). The G_{20} cell displayed three thick primary dendrites from which up to fifth-order branches emerged to from a bistratified arbor (28% and 51% depths of the IPL) (Figs. 12A–C, 13). Both primary and higher-order dendrites were very wavy and displayed many swellings. Interestingly, while sublamina-b contained both lower order dendrites and terminal branches, sublamina-a was populated mostly by terminal dendrites (Fig. 12B,C). The G_{20} cell resembled most monostratified cluster 4 cells of Badea and Nathans (2004) and somewhat cells in cluster M13 of Coombs et al. (2006).

The G_{20} cell displayed heterologous coupling to six small (≈5 μm diameter) amacrine cell somata in the INL (Fig. 12D), whose labels were confined to their somata making further morphological examination impossible.

G_{21} ganglion cell (n = 1)—The G_{21} cell displayed a medium-sized cell body (≈15 μm in diameter) and dendritic arbor (≈162 μm) that bistratified at the 66% and 84% depths of the IPL. While the dendritic architecture of the G_{21} cell resembled that of the G_{20} ganglion cell, it had stouter and significantly straighter dendrites and displayed fewer dendritic swellings (Figs. 12E–G, 13). Morphological features of the G_{21} cell resembled cells in monostratified cluster 5 of Badea and Nathans (2004) and cells in cluster M13 of Coombs et al. (2006).

The G_{21} cell displayed heterologous coupling to four amacrine cells with cell bodies displaced to the GCL (Fig. 12E). Labeling of these coupled amacrine cells was confined to their cell bodies and thus further morphological examination was not possible.

G_{22} ganglion cell (n = 1)—The G_{22} cell displayed a medium-sized soma (≈17 μm diameter) and small dendritic arbor (≈122 μm diameter) (Figs. 12H–J, 13) that bistratified at

the 37% and 57% depths of the IPL. The G_{22} cell displayed seven relatively thin primary dendrites from which wavy higher segments emerged that showed numerous swellings. The G_{22} cell shared many morphological features with bistratified cluster 1 and 2 cells of Badea and Nathans (2004) and M12, M13, and M14 cluster cells of Coombs et al. (2006). The G_{22} ganglion cell showed no evidence of tracer coupling.

DISCUSSION

Morphological characterization of mouse ganglion cells

In this study we injected 210 ganglion cells with Neurobiotin to reveal the soma/dendritic morphology of the distinct sub-types in the wildtype mouse retina. Using a number of morphometric features, we distinguished 22 subpopulations of ganglion cells (summarized in Fig. 13) and then determined the tracer coupling of each (Table 1). It is important to note that the coupling pattern of a ganglion cell was never used to classify it and thus was treated as a variable independent of a cell's morphological identity. Still, we found that the tracer coupling pattern of each distinct ganglion cell subpopulation was stereotypic across the dark-adapted retinas we studied.

A number of previous studies, using a variety of morpho-metric methods, have described the different ganglion cell subtypes in the mouse retina. Although we classified our cells independent of these studies, they still form important frameworks in which to compare and incorporate our ganglion cell subtypes (Table 2). Sun et al. (2002) initially characterized 17 ganglion cell subtypes using classical morphological criteria including soma and dendritic size, soma/dendritic architecture, and dendritic stratification in the IPL. Three subsequent studies used cluster analyses to sort murine ganglion cells in a multidimensional space. These studies distinguished 12 (Badea and Nathans, 2004), 11 (Kong et al., 2005), and 19 (Coombs et al., 2006) distinct ganglion cell morphological clusters. Overall, 17 of our 22 ganglion cell subtypes could be clearly matched to the 17 ganglion cell subpopulations characterized by Sun et al. (2002). The remaining five subtypes appear to be rare ganglion cells that were not encountered in the Sun et al. (2002) study. In addition, most of our ganglion cell subtypes were described in the cluster analysis studies, including four subtypes which had no counterparts in the description by Sun et al. (2002). However, whereas we found one-to-one correlations between 17 of our ganglion cell sub-types with those described by Sun et al. (2002), the relationship of our cells to those reported in the cluster analysis studies was more equivocal. First, some of our ganglion cell subtypes appeared to match cells in more than one cluster. For example, the G_5 cells resembled ganglion cells in both monostratified 2 and monostratified 4 clusters of Badea and Nathans (2004). Second, a number of our ganglion cell sub-types did not appear to be included in one or more of these clustering schemes. Our G_{19} ganglion cell had no counterpart in any of the previous studies. Third, cells in certain clusters resembled more than one of our ganglion cell subpopulations. For example, descriptions of cluster 1 cells in the scheme provided by Kong et al. (2005) resembled G_5,G_8, and G_{13} cells in our sample. This disparity between the different datasets, including our own, is likely due to the different labeling and analyzing techniques, but also suggests that some clusters incorporate multiple ganglion cell subtypes. It should be noted that some of our morphometric values (e.g., soma size, dendritic fields diameter) were 25–50% smaller than those given for counterpart ganglion cell subtypes in the previous studies (Sun et al., 2002; Badea and Nathans, 2004; Kong et al., 2005; Coombs et al., 2006). This discrepancy is most likely due to tissue shrinkage resulting from the dehydration process in our histological protocol.

Tracer-coupling patterns of mouse ganglion cells

This article is the first comprehensive study to describe and compare ganglion cell coupling across the entire population in the wildtype mouse retina. Overall, our study indicates that the different ganglion cell subtypes display stereotypic tracer coupling patterns in the mouse retina (summarized in Fig. 14). Thus, the tracer coupling pattern can be a useful and additional feature to distinguish the different ganglion cell sub-types. However, it is important to point out that, despite the standardized experimental conditions used here, we did observe some variability in the absolute number of cells coupled to ganglion cells of the same subtype (see Table 1). While this observation may reflect biological variability, we believe it more likely reflects a technical variability related to inconsistency in the amount of tracer delivered via electrodes and its diffusion across the coupled network of cells. Despite this variability in the absolute number of coupled cells, the overall coupling pattern remained stereotypic for each ganglion cell subtype.

We found that 16 of the 22 morphologically distinct ganglion cell subpopulations displayed homologous coupling to ganglion cell neighbors and/or heterologous coupling to nearby amacrine cells. Although varied, we found that the ganglion cell coupling in the mouse retina was governed by some general rules. First, ON ganglion cells were coupled to amacrine cells with somata displaced to the GCL, whereas OFF ganglion cells were coupled to amacrine cells with somata lying in the INL. Second, most ON ganglion cells were coupled to polyaxonal amacrine cells (G_1,G_6, and G_{10}; but not G_2), whereas OFF ganglion cells were coupled to wide-field amacrine cells (G_3 and G_7). Third, homologous ganglion-toganglion cell coupling occurred only among cells whose dendrites stratified at least partially in sublamina-a, which included ganglion cells with diffuse (G_{13} cells), monostratified (G_3,G_6,G_{11}, and G_{18} cells) and bistratified dendritic arbors (G_{16} and G_{17} cells). These are presumably OFF and ON-OFF physiological subtypes. Ganglion cells whose dendritic arbor was restricted to sublamina-b, presumably ON cells, never showed homologous coupling. Fourth, of the ganglion cells that showed homologous coupling, only bistratified ganglion cells (G_{16} and G_{17} cells) were not coupled to amacrine cells as well.

We found that seven ganglion cell populations displayed homologous coupling with their ganglion cell neighbors. In many G_3,G_7,G_{17}, and G_{18} cell injections, not only somata, but proximal dendrites or even the entire dendritic arbor of homologously coupled ganglion cells were visible as well. In all these cases, soma/dendritic morphologies of coupled and injected ganglion cells were identical. This finding indicates that mouse ganglion cells only couple to nearby like-type ganglion cells. However, it remains to be determined if inter-typical coupling can also be ruled out for G_{11},G_{13}, and G_{16} cells where labels were confined to coupled somata.

We found that 14 ganglion cell populations showed heterologous coupling to amacrine cells, whose arbors were often visible, allowing for examination of their soma/dendritic morphologies. Interestingly, all coupled amacrine cells observed in this study were either polyaxonal or wide-field amacrine cells, whereas we found no evidence of coupling between ganglion cells and narrow-field amacrine cells. However, labels of many coupled amacrine cells were restricted to their soma and yet to be morphologically characterized.

Role of ganglion cell coupling

Overall, our results indicate that nearly three-quarters of the ganglion cells in the mouse retina are coupled to ganglion cell and/or amacrine cell neighbors. This extensive coupling in the inner mouse retina is consistent with findings in other mammals (Vaney, 1991, 1994; Xin and Bloomfield, 1997; Hoshi et al., 2007). At first glance, this widespread coupling is disconcerting, as it suggests a significant lateral spread of visual signals as they leave the

retina, thereby substantially reducing spatial acuity and blurring the image transmitted to higher visual centers. However, previous morphological studies have shown that the tracer coupling patterns of ganglion cells are restricted to small local groups of nearest neighbors (Vaney, 1991, 1994; Xin and Bloomfield, 1997). This circumscribed pattern of tracer movement was particularly true for the homologous coupling we observed here for murine ganglion cells. Likewise, the receptive fields of individual ganglion cells have been shown to match closely the size of their dendritic fields, irrespective of the presence of tracer coupling (Bloom-field and Xin, 1997; Völgyi et al., 2000). Taken together, these results suggest that electrical synapses formed by ganglion cells do not underlie a significant spread of current across the IPL, and thus their function must be quite different from that of the extensively coupled horizontal cell syncytia in the outer retina.

One proposed function for ganglion cell electrical coupling is to provide for correlated activity of neighboring cells. Correlated firing is believed to compress information for efficient transmission and thereby enhance bandwidth of the optic nerve (Meister and Berry, 1999). In this scheme, synchronous activity can provide additional information to the brain by multiplexing with asynchronous signals from individual ganglion cells. Concerted spike activity is also thought to enhance the saliency of visual signals by increasing temporal summation at central targets (Alonso et al., 1996; Stevens and Zador, 1998; Usrey and Reid, 1999). In this way, concerted ganglion cell activity may provide the temporal precision by which retinal signals are reliably transmitted to central targets (Singer, 1999). In fact, correlated spiking may account for up to one-half of all retinal spike activity, largely a result of the extensive coupling between ganglion and amacrine cells in the IPL.

Concerted activity among ganglion cells can range from relatively loose correlations, reflected in cross-correlograms spanning tens of milliseconds, to narrowly synchronized spikes with latencies <3 msec (Arnett and Spraker, 1981; Mastronarde, 1983a–c; Brivanlou et al., 1998; DeVries, 1999; Hu and Bloomfield, 2003). The short latency correlations are believed to reflect direct electrical coupling between neighboring ganglion cells, whereas the somewhat broader intermediate correlations may be generated by ganglion cells forming electrical synapses with a common population of amacrine cells (Brivanlou et al., 1998; DeVries, 1999; Hu and Bloomfield, 2003). Interestingly, we found that about one-third of our ganglion cell subtypes displayed homologous coupling to their neighbors, whereas nearly two-thirds showed heterologous coupling to amacrine cells. Our results thus suggest that a range of concerted spike activity for ganglion cells is present in the mouse retina, but intermediate latency correlations should be the most prevalent. This idea is consistent with the findings Schnitzer and Meister (2003) indicating that the intermediate latency correlation is the most common form of concerted spiking in the vertebrate retina. Clearly, physiological studies are called for to examine the concerted activity of murine ganglion cells to elucidate the functional roles of the different patterns of coupling expressed in the IPL of the mouse retina.

Acknowledgments

Grant sponsor: National Institutes of Health (NIH); Grant numbers: EY017832 (to B.V.) and EY07360 to (S.A.B.).

LITERATURE CITED

Alonso JM, Usrey WM, Reid RC. Precisely correlated firing in cells of the lateral geniculate nucleus. Nature. 1996; 383:815–819. [PubMed: 8893005]

Arnett D, Spraker TE. Cross-correlation analysis of the maintained discharge of rabbit retinal ganglion cells. J Physiol. 1981; 317:29–47. [PubMed: 7310736]

Badea TC, Nathans J. Quantitative analysis of neuronal morphologies in the mouse retina visualized by using a genetically directed reporter. J Comp Neurol. 2004; 480:331–351. [PubMed: 15558785]

Baldridge WH, Vaney DI, Weiler R. The modulation of intercellular coupling in the retina. Semin Cell Dev Biol. 1998; 9:311–318. [PubMed: 9665867]

Bloomfield SA, Miller RF. A physiological and morphological study of the horizontal cell types of the rabbit retina. J Comp Neurol. 1982; 208:288–303. [PubMed: 6288777]

Bloomfield SA, Völgyi B. Function and plasticity of homologous coupling between AII amacrine cells. Vision Res. 2004; 44:3297–3306. [PubMed: 15535997]

Bloomfield SA, Xin D. A comparison of receptive-field and tracer-coupling size of amacrine and ganglion cells in the rabbit retina. Vis Neurosci. 1997; 14:1153–1165. [PubMed: 9447695]

Bloomfield SA, Xin D, Osborne T. Light-induced modulation of coupling between AII amacrine cells in the rabbit retina. Vis Neurosci. 1997; 14:565–576. [PubMed: 9194323]

Boycott BB, Wässle H. The morphological types of ganglion cells of the domestic cat's retina. J Physiol Lond. 1974; 286:397–419. [PubMed: 4422168]

Brivanlou IH, Warland DK, Meister M. Mechanisms of concerted firing among retinal ganglion cells. Neuron. 1998; 20:527–539. [PubMed: 9539126]

Bunt AH. Ramification patterns of ganglion cell dendrites in the retina of the albino rat. Brain Res. 1976; 103:1–8. [PubMed: 56206]

Chang B, Hawes NL, Hurd RE, Wang J, Howell D, Davisson MT, Roderick TH, Nusinowitz S, Heckenlively JR. Mouse models for ocular diseases. Vis Neurosci. 2005; 22:587–593. [PubMed: 16332269]

Coombs J, Van Der List D, Wang G-Y, Chalupa LM. Morphological properties of mouse retinal ganglion cells. Neuroscience. 2006; 140:123–136. [PubMed: 16626866]

Dacey DM, Brace S. A coupled network for parasol but not midget ganglion cells in the primate retina. Vis Neurosci. 1992; 9:279–290. [PubMed: 1390387]

Deans MR, Völgyi B, Goodenough DA, Bloomfield SA, Paul DL. Connexin36 is essential for transmission of rod-mediated visual signals in the mammalian retina. Neuron. 2002; 36:1–20. [PubMed: 12367498]

DeVries SH. Correlated firing in rabbit retinal ganglion cells. J Neurophysiol. 1999; 81:908–920. [PubMed: 10036288]

Famiglietti EV. Polyaxonal amacrine cells of rabbit retina: morphology and stratification of PA1 cells. J Comp Neurol. 1992a; 316:391–405. [PubMed: 1577992]

Famiglietti EV. Polyaxonal amacrine cells of rabbit retina: PA2, PA3, and PA4 cells. Light and electron microscopic studies with a functional interpretation. J Comp Neurol. 1992b; 316:422–446. [PubMed: 1374438]

Feigenspan A, Teubner B, Willecke K, Weiler R. Expression of neuronal connexin36 in AII amacrine cells of the mammalian retina. J Neurosci. 2001; 21:230–239. [PubMed: 11150340]

Güldenagel M, Ammermüller J, Feigenspan A, Teubner B, Degen J, Söhl G, Willecke K, Weiler R. Visual transmission deficits in mice with targeted disruption of the gap junction gene connexin36. J Neurosci. 2001; 21:6036–6044. [PubMed: 11487627]

He S, Weiler R, Vaney DI. Endogenous dopaminergic regulation of horizontal cell coupling in the mammalian retina. J Comp Neurol. 2000; 418:33–40. [PubMed: 10701754]

Hidaka S, Akahori Y, Kurosawa Y. Dendrodendritic electrical synapses between mammalian retinal ganglion cells. J Neurosci. 2004; 24:10553–10567. [PubMed: 15548670]

Hombach S, Janssen-Bienhold U, Sohl G, Schubert T, Bussow H, Ott T, Weiler R, Willecke K. Functional expression of connexin57 in horizontal cells of the mouse retina. Eur J Neurosci. 2004; 19:2633–2640. [PubMed: 15147297]

Hoshi H, Kim I-B, Mills SL. The incidence of ganglion cell coupling in the rabbit retina. Invest Ophthalmol Vis Sci. 2007; 48(Suppl):1161.

Hu EH, Bloomfield SA. Gap junctional coupling underlies the short-latency spike synchrony of retinal α ganglion cells. J Neurosci. 2003; 23:6768–6777. [PubMed: 12890770]

Hu EH, Dacheux RF, Bloomfield SA. A flattened retina-eyecup preparation suitable for electrophysiological studies of neurons visualized with trans-scleral infrared illumination. J Neurosci Methods. 2000; 103:209–216. [PubMed: 11084214]

Huxlin KR, Goodchild K. Retinal ganglion cells in the albino rat: revised morphological classification. J Comp Neurol. 1997; 385:309–323. [PubMed: 9268130]

Jeon CJ, Strettoi E, Masland RH. The major cell populations of the mouse retina. J Neurosci. 1998; 18:8936–8946. [PubMed: 9786999]

Kim IJ, Zhang Y, Yamagata M, Meister M, Sanes JR. Molecular identification of a retinal cell type that responds to upward motion. Nature. 2008; 452:478–482. [PubMed: 18368118]

Kong J-H, Fish DR, Rockhill RL, Masland RH. Diversity of ganglion cells in the mouse retina: unsupervised morphological classification and its limits. J Comp Neurol. 2005; 489:293–310. [PubMed: 16025455]

Lin B, Masland RH. Populations of wide-field amacrine cells in the mouse retina. J Comp Neurol. 2006; 499:797–809. [PubMed: 17048228]

Mastronarde DN. Correlated firing of cat retinal ganglion cells. I. Sponteneously active inputs to X- and Y-cells. J Neurophysiol. 1983a; 49:303–324. [PubMed: 6300340]

Mastronarde DN. Correlated firing of cat retinal ganglion cells. II. Responses of X- and Y-cells to single quantal events. J Neurophysiol. 1983b; 49:325–349. [PubMed: 6300341]

Mastronarde DN. Interactions between ganglion cells in the cat retina. J Neurophysiol. 1983c; 49:350–365. [PubMed: 6300342]

Maxeiner S, Dedek K, Janssen-Bienhold U, Ammermuller J, Brune H, Kirsch T, Pieper M, Degen J, Kruger O, Willecke K, Weiler R. Deletion of connexin45 in mouse retinal neurons disrupts the rod/cone signaling pathway between AII amacrine and ON cone bipolar cells and leads to impaired visual transmission. J Neurosci. 2005; 25:566–576. [PubMed: 15659592]

Meier C, Dermietzel R. Electrical synapses — gap junctions in the brain. Results Probl Cell Differ. 2006; 43:99–128. [PubMed: 17068969]

Meister M, Berry MJ. The neural code of the retina. Neuron. 1999; 22:435–450. [PubMed: 10197525]

Meister M, Legnado L, Baylor DA. Correlated signaling by retinal ganglion cells. Science. 1995; 270:1207–1210. [PubMed: 7502047]

Mills SL, Massey SC. Differential properties of two gap junctional pathways made by AII amacrine cells. Nature. 1995; 377:734–737. [PubMed: 7477263]

Mills SL, O'Brien JJ, Li W, O'Brien J, Massey SC. Rod pathways in the mammalian retina use connexin 36. J Comp Neurol. 2001; 436:336–350. [PubMed: 11438934]

Penn AA, Wong RO, Shatz CJ. Neuronal coupling in the developing mammalian retina. J Neurosci. 1994; 14:3805–3815. [PubMed: 8207489]

Peichl L. Alpha and delta ganglion cells in the rat retina. J Comp Neurol. 1989; 286:120–139. [PubMed: 2768556]

Peichl L, Buhl EH, Boycott BB. Alpha ganglion cells in the rabbit retina. J Comp Neurol. 1987a; 263:25–41. [PubMed: 2444630]

Peichl L, Ott H, Boycott BB. Alpha ganglion cells in mammalian retinae. Proc R Soc Lond B. 1987b; 231:169–197. [PubMed: 2889210]

Pérez De Sevilla Müller L, Shelley J, Weiler R. Displaced amacrine cells of the mouse retina. J Comp Neurol. 2007; 505:177–189. [PubMed: 17853452]

Schnitzer MJ, Meister M. Multineuronal firing patterns in the signal from eye to brain. Neuron. 2003; 37:499–511. [PubMed: 12575956]

Schubert T, Degen J, Willwcke K, Hormuzdi SG, Monyer H, Weiler R. Connexin36 mediates gap junctional coupling of alpha-ganglion cells in mouse retina. J Comp Neurol. 2005a; 485:191–201. [PubMed: 15791644]

Schubert T, Maxeiner S, Kruger O, Willecke K, Weiler R. Connexin45 mediates gap junctional coupling of bistratified ganglion cells in the mouse retina. J Comp Neurol. 2005b; 490:29–39. [PubMed: 16041717]

Shelley J, Dedek K, Schubert T, Feigenspan A, Schultz K, Hombach S, Willecke K, Weiler R. Horizontal cell receptive fields are reduced in connexin57-deficient mice. Eur J Neurosci. 2006; 23:3176–3186. [PubMed: 16820008]

Singer W. Neuronal synchrony: a versatile code for the definition of relations? Neuron. 1999; 24:49–65. [PubMed: 10677026]

Stafford DK, Dacey DM. Physiology of the A1 amacrine: a spiking, axon-bearing interneuron of the macaque monkey retina. Vis Neurosci. 1997; 14:507–522. [PubMed: 9194317]

Stanford LR, Sherman SM. Structure/function relationships of retinal ganglion cells in the cat. Brain Res. 1984; 297:381–386. [PubMed: 6326945]

Stevens CF, Zador AM. Input synchrony and the irregular firing of cortical neurons. Nat Neurosci. 1998; 1:210–207. [PubMed: 10195145]

Sun W, Li X, He S. Large-scale morphological survey of mouse retinal ganglion cells. J Comp Neurol. 2002; 451:115–126. [PubMed: 12209831]

Usrey WM, Reid RC. Synchronous activity in the visual system. Annu Rev Physiol. 1999; 61:435–456. [PubMed: 10099696]

Vaney DI. Many diverse types of retinal neurons show tracer coupling when injected with biocytin or Neurobiotin. Neurosci Lett. 1991; 125:187–190. [PubMed: 1715532]

Vaney DI. Territorial organization of direction-selective ganglion cells in rabbit retina. J Neurosci. 1994; 14:6301–6316. [PubMed: 7965037]

Völgyi B, Bloomfield SA. Effects of GABA blockers on the response properties of amacrine and ganglion cells in the rabbit retina. Invest Ophthalmol Vis Neurosci. 2000; 41(Suppl):3286.

Völgyi B, Xin D, Amarillo Y, Bloomfield SA. Morphology and physiology of the polyaxonal amacrine cells in the rabbit retina. J Comp Neurol. 2001; 440:109–125. [PubMed: 11745611]

Völgyi B, Deans MR, Paul DL, Bloomfield SA. Convergence and segregation of the multiple rod pathways in mammalian retina. J Neurosci. 2004; 24:11182–11192. [PubMed: 15590935]

Völgyi B, Abrams J, Paul DL, Bloomfield SA. Connexin36 comprises heterologous but not homologous gap junctions formed by alpha ganglion cells in mouse retina. Invest Ophthalmol Vis Neurosci. 2005a; 46(Suppl):2231.

Völgyi B, Abrams J, Paul DL, Bloomfield SA. Morphology and tracer coupling pattern of alpha ganglion cells in the mouse retina. J Comp Neurol. 2005b; 492:66–77.

Weiler R, Pottek M, He S, Vaney DI. Modulation of coupling between retinal horizontal cells by retinoic acid and endogenous dopamine. Brain Res Brain Res Rev. 2000; 32:121–129. [PubMed: 10751661]

Xin D, Bloomfield SA. Tracer coupling pattern of amacrine and ganglion cells in the rabbit retina. J Comp Neurol. 1997; 383:512–528. [PubMed: 9208996]

Xin D, Bloomfield SA. Dark- and light-induced changes in coupling between horizontal cells in mammalian retina. J Comp Neurol. 1999; 405:75–87. [PubMed: 10022197]

Xin D, Bloomfield SA. Effects of nitric oxide on horizontal cells in the rabbit retina. Vis Neurosci. 2000; 17:799–811. [PubMed: 11153659]

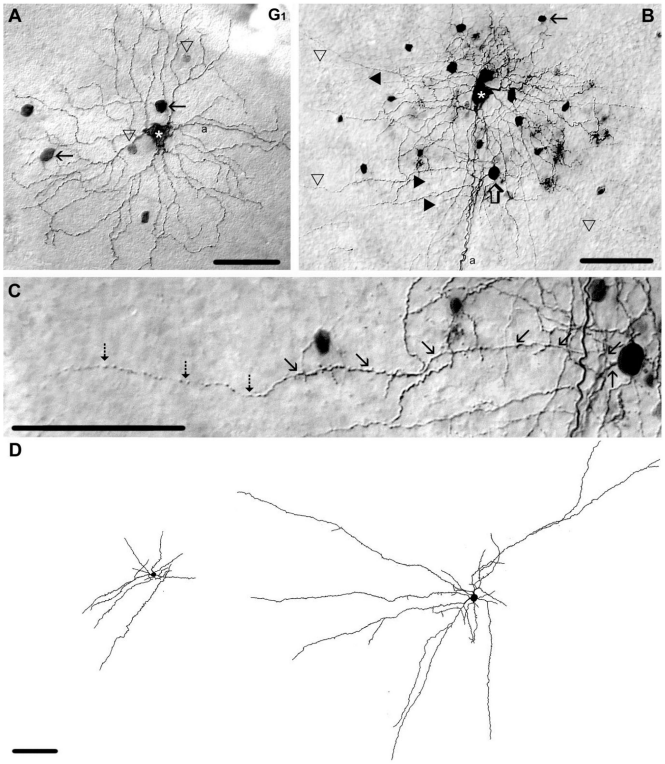

Figure 1.

Morphology and tracer coupling pattern of the G_1 ganglion cell subtype in the mouse retina. A: Photomicrograph showing the soma/dendritic morphology of a Neurobiotin-injected G_1 cell with a large soma (asterisk) and five primary dendrites that branch relatively close to the soma. This G_1 cell shows tracer-coupling to small (arrowhead) and large (arrow) amacrine cells with somata displaced to the GCL. B: This other G_1 cell (white asterisk) displays intensive tracer coupling to neighboring amacrine cells. The arrow points to the small amacrine cell drawn in D left, whereas the open arrow points to the soma of a large coupled amacrine cell drawn in D right. Tracer-coupled amacrine cells display both dendritic (filled arrowhead) and axonal (open arrowhead) processes. C: High-power photomicrograph showing a selected area of panel B, where one process of a selected coupled amacrine cell (open arrow in panel B) is traced by arrows. Note that an axon (dashed arrows) emerges from the tip of this dendrite. D: Camera-lucida drawing shows morphologies of tracer coupled amacrine cells marked by arrow and open arrow in panel B. These tracer-coupled amacrine cells display both dendritic and axonal processes. Note that, due to limited tracer diffusion into coupled cells, these drawings show only the proximal arbor of the amacrine cells. a, axon. Scale bars = 100 μm.

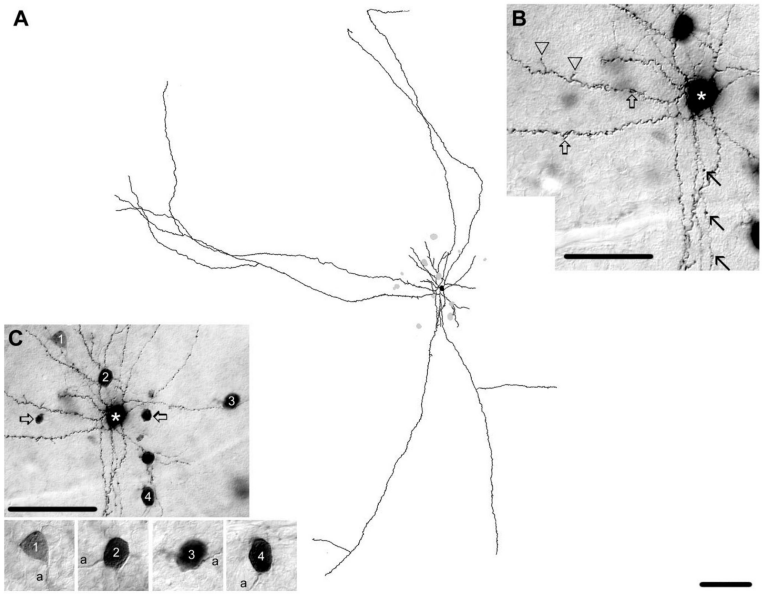

Figure 2.

Morphology of a polyaxonal amacrine cell tracer coupled to G_1 ganglion cells. A: Camera-lucida drawing shows the entire dendritic/axonal arbor of a Neurobiotin-injected polyaxonal amacrine cell with soma/dendritic morphology similar to those coupled to G_1 ganglion cells. Gray somata represent cells that appear coupled to this Neurobiotin-injected polyaxonal cell. B: High-magnification micrograph showing dendritic specializations of the injected polyaxonal cell (asterisk). Dendrites display relatively large swellings (open arrows) and spines (arrowheads), whereas axons display small swellings at regular distances (arrows). C: Photomicrograph showing the proximal soma/dendritic region of the injected polyaxonal cell drawn in panel A; asterisk marks the injected soma. This amacrine cell shows coupling to amacrine cells (open arrows) and ganglion cells (1–4 here and in insets) whose soma size and shape resemble those of G_1 ganglion cells. a, axon. Scale bars = 100 μm in A–C; 50 μm in C insets.

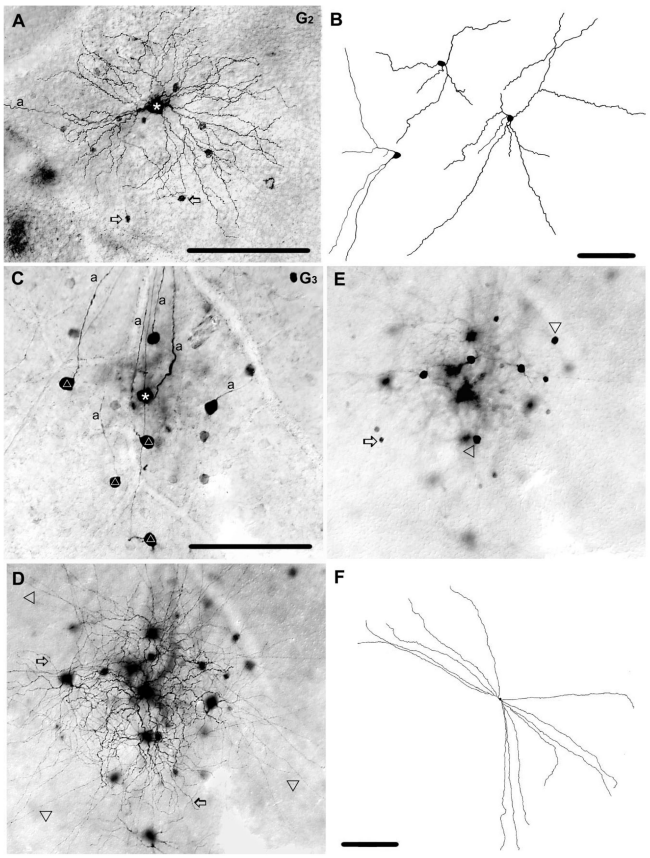

Figure 3.

Morphology and tracer coupling patterns of the G_2 and G_3 ganglion cell subtypes. A: Photomicrograph displaying the soma/dendritic morphology of a Neurobiotin-injected G_2 cell (asterisk). This G_2 cell displays tracer-coupling to a subset of amacrine cells with somata displaced to the GCL (open arrows). B: Camera-lucida drawings show soma/dendritic morphologies of three amacrine cells that are coupled to G_2 cells; note that a limited tracer-flow confined the labels of these cells to their proximal dendritic arbor. C: Photomicrograph of a Neurobiotin-injected G_3 cell (asterisk) displaying homologous tracer-coupling to an array of neighboring ganglion cells (triangles). D: Same frame as in panel C, but with focal plane on the dendrites of both injected and coupled ganglion cells (arrows) in the IPL. Arrowheads point to long, straight radial running dendrites of coupled amacrine cells that costratify with G_3 cell dendrites. E: Photomicrograph showing the frames in panels C,D, but with focal depth at the somata of coupled amacrine cells in the INL. Arrows and arrowheads point to small and large tracer-coupled amacrine cells, respectively. F: Camera-lucida drawing shows the entire dendritic arbor of a wide-field amacrine cell that is coupled to G_3 ganglion cells. a. axon. Scale bars = 100 μm in A–E; 200 μminF.

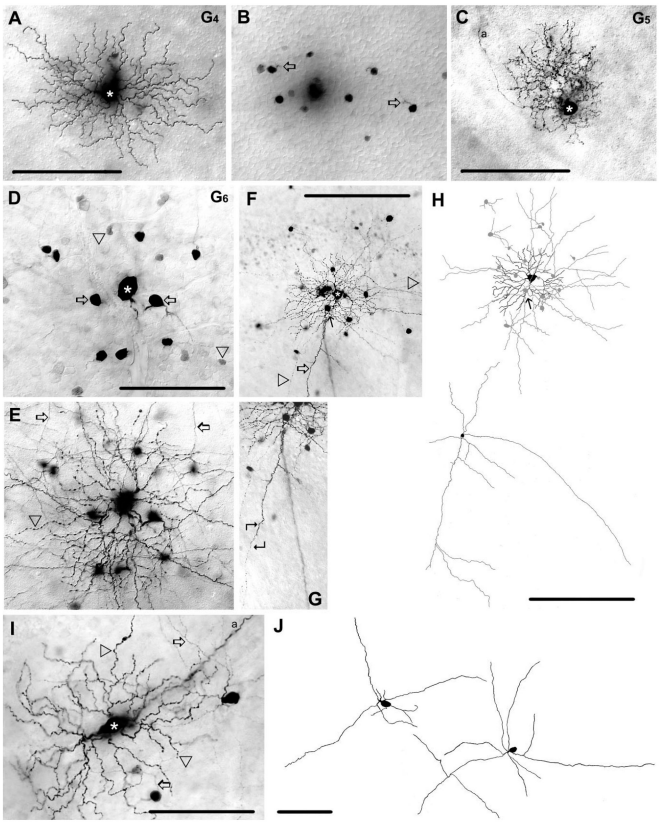

Figure 4.

Morphology and tracer coupling pattern of the G_4,G_5, and G_6 ganglion cells. A: Photomicrograph showing a G_4 ganglion cell (asterisk) with medium-sized dendritic arbor. B: Same frame as in panel A, but with focal depth at the level of the proximal INL. The G_4 cell is tracer coupled to amacrine cells with somata that lay in the INL; primary dendrites are indicated by open arrows. C: Photomicrograph showing a tracer-injected G_5 ganglion cell (asterisk). This G_5 cell displays a dense, bushy dendritic arbor, but shows no evidence of tracer coupling. D: Photomicrograph showing a Neurobiotin-injected G_6 ganglion cell (asterisk). This cell displays heterologous coupling to small (arrowheads) and large (arrows) amacrine cell somata displaced to the GCL. E: Photomicrograph shows the same frame as in D, but with focus on the dendritic processes (arrowhead) of the injected G_6 cell. Arrows point to amacrine cell processes costratifying with dendrites of the injected G_6 cell. F: Photomicrograph of another G_6 cell (asterisk) showing that coupled amacrine cells display both thick dendritic (arrow) and thin axonal (arrowheads) processes. Filled arrow (here and in panel H top) points to the amacrine cell whose dendrite is magnified in panel G and drawn in panel H bottom. G: A selected area of panel F is magnified to show the proximal soma/dendritic region of a coupled amacrine cell (filled arrows in panels F and H top). Angled arrows frame the area where a characteristic dendrite/axon transition occurs. H: Top panel shows a camera-lucida drawing of the G_6 ganglion cell (black) shown in panel F as well as somata and processes of coupled amacrine cells (gray). Lower panel shows the proximal dendritic/ axonal arbor of the coupled amacrine cell marked in panels F,H top (arrow). Note that due to a limited tracer flow into coupled cells this drawing shows only a portion of their arbor. I: AG_6 ganglion cell whose soma is elongated, but otherwise shares all other features of G_6 cells. Arrowheads label injected ganglion cell dendrites, whereas arrows point to dendritic processes of coupled amacrine cells. J: Camera-lucida drawings display cell bodies and proximal dendritic/axonal areas of amacrine cells coupled to elongated G_6

ganglion cells. Soma/ dendritic morphology of these amacrine cells are identical to amacrine cells coupled to other G_6 ganglion cells (see panels D–H). Note that due to a limited tracer flow into coupled cells this drawing shows only a portion of their arbor. a, axonal process. Scale bars = 100 μmin A–E,I–J; 200 μm in F,H; 150 μminG.

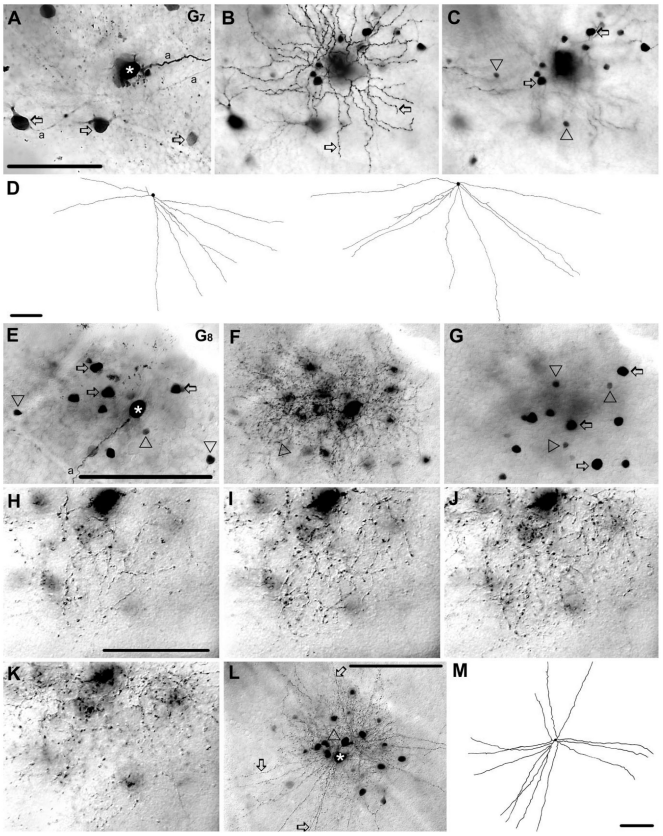

Figure 5.

Morphology and tracer coupling pattern of the G_7 and G_8 ganglion cell subtypes in the mouse retina. A: Photomicrograph showing a G_7 cell (asterisk) homologously coupled to other ganglion cells in the GCL (arrows). B,C: Panels focusing on the dendrites (arrows) of the injected G_7 cell in the IPL (B) and on the somata of heterologously coupled amacrine cells in the INL (C). Arrows and arrowheads in C point to coupled amacrine cells with large and small cell bodies, respectively. D: Camera-lucida drawings show the entire dendritic arbors of amacrine cells coupled to G_7 cells, which show long, straight dendrites that branch only proximally. E–G: Photomicrographs of a G_8 cell focusing on the GCL (E), IPL (F), and the INL (G). Asterisk in E marks the injected soma, whereas arrows and arrowheads point to large and small somata of coupled amacrine cells in the GCL, respectively. Arrowhead in panel F points to one of many delicate G_8 cell dendrites. Arrows and arrowheads in panel G point to large and small somata of coupled amacrine cells in the INL, respectively. H–K: High-magnification photomicrographs of a selected dendritic area of a G_8 ganglion cell with focuses on four consecutive planes at 80% 65%, 50%, and 35% depths of the IPL. All planes contain dendritic terminals indicating that the arbor of this G_8 cell stratifies diffusely. L: Another G_8 cell (asterisk) coupled to an amacrine cell (arrowhead) with long and straight radiate dendrites (arrows). M: Camera-lucida drawing shows the entire dendritic arbor of the coupled wide-field amacrine cell marked in L. a, axon. Scale bars = 100 μm in A–G,L,M; 40 μmin H–K.

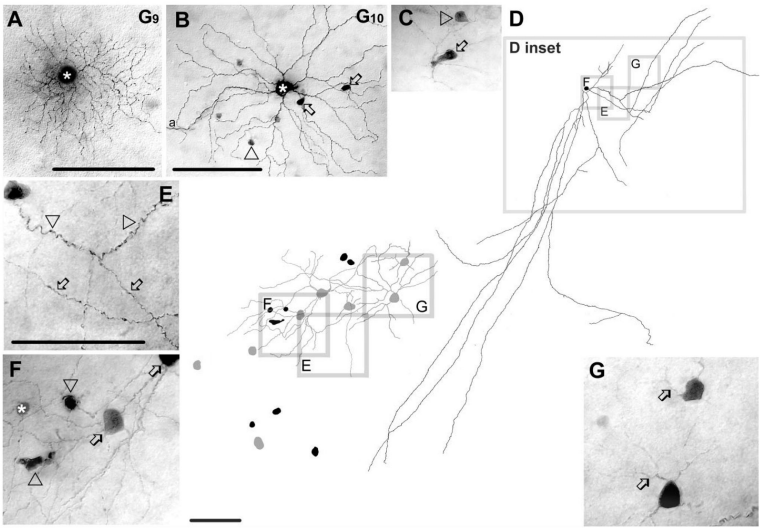

Figure 6.

Morphology and tracer coupling pattern of the G_9 and G_{10} ganglion cells. A: Photomicrograph of a G_9 cell (asterisk) with relatively dense branching and medium-sized dendritic arbor. This G_9 cell shows no evidence of tracer coupling. B: AG_{10} cell (asterisk) that is coupled to amacrine cells with somata displaced into the GCL. Somata of these coupled amacrine cells were either round (arrowhead) or elongated (arrows). C: High-magnification image shows cell bodies of two amacrine cells coupled to G_{10} cells, which display elongated (arrow) and spherical (arrowhead) cell bodies. D: Camera-lucida drawing shows the entire dendritic/axonal arbor of a Neurobiotin-injected polyaxonal amacrine cell whose soma/dendritic morphology resemble the amacrine cells coupled to G_{10} ganglion cells (right); D inset specifies areas that are enlarged (left). This latter drawing shows cell bodies of coupled amacrine (black) and ganglion cells (gray). Frames E–G in both D right and D left mark areas enlarged in corresponding E–G photomicrographs. E: This image shows wavy dendritic (arrowheads) and beaded axonal (arrows) processes of the injected polyaxonal amacrine cell. F: Enlarged image showing the injected amacrine cell soma (asterisk), spherical and elongated coupled amacrine cell somata (arrowheads) and heterologously coupled ganglion cell somata (arrows). Coupled amacrine cell somata are similar to those amacrine cells that are coupled to injected G_{10} cells, whereas the coupled ganglion cells resemble G_{10} cells shown in panels B and C. G: Two coupled ganglion cells showing relatively long bifurcating primary dendrites (arrows) characteristic of G_{10} cells. a, axon. Scale bars = 100 μm in A,B,D right, E–G; 30 μminC;140 μm in D left.

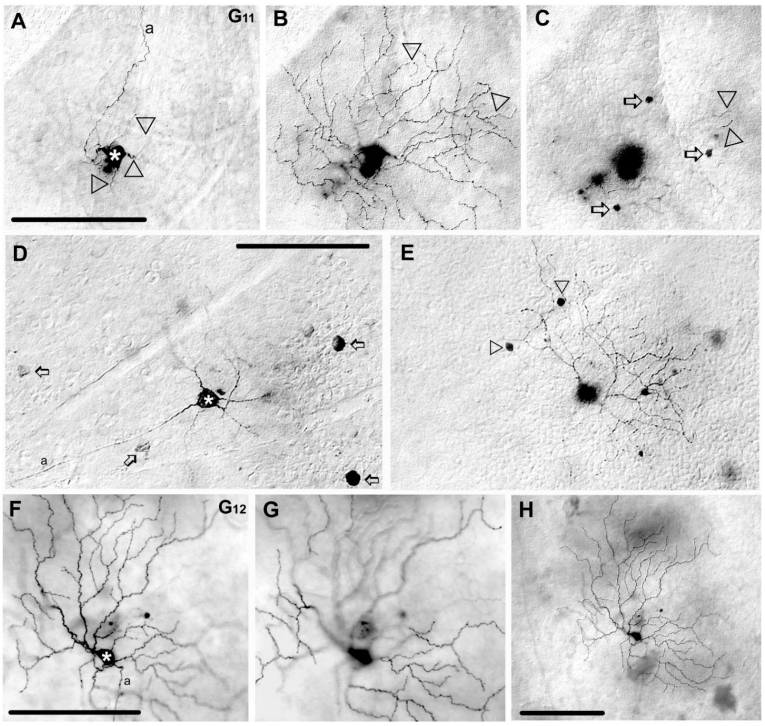

Figure 7.

Morphology and tracer coupling pattern of the G_{11} and G_{12} ganglion cell subtypes in the mouse retina. A: Photomicrograph shows the soma (asterisk) and primary dendrites (arrowheads) of a Neurobiotin-injected G_{11} cell. B: Photomicrograph showing the same injected G_{11} cell as in panel A with focus on the dendrites in sublamina-a of the IPL; arrowheads point to circumflexed dendritic endings. C: Photomicrograph focusing on the INL showing that this G_{11} cell displays heterologous coupling to small amacrine cells with somata in the INL (arrows). Some dendritic tips (arrowheads) of the injected G_{11} cell appear in this frame near to the IPL/INL border. D,E: Photomicrographs showing another labeled G_{11} cell (asterisk). Unlike the G_{11} cell in panel A, this cell displays homologous coupling to neighboring ganglion cells (arrows), whereas it shares all other features with other G_{11} cells including dendritic morphology, stratification of dendrites, and coupling to amacrine cells with small somata (arrowheads) in the INL. F,G: Pair of photomicrographs showing a tracer-injected G_{12} cell (asterisk) with dendrites stratifying either in sublamina-b (F) or sublamina-a (G). H: A low-power photomicrograph of the same G_{12} cell showing that this ganglion cell is entirely uncoupled. a, axon. Scale bars = 100 μm.

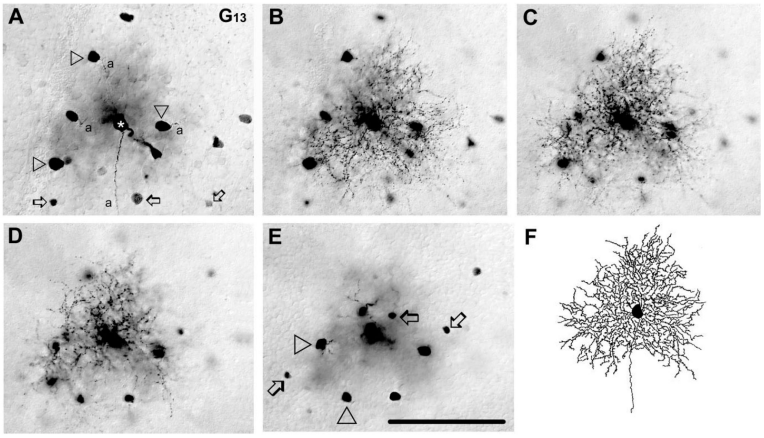

Figure 8.

Morphology and tracer coupling pattern of G_{13} ganglion cells. A–E: Photomicrographs showing a G_{13} cell (asterisk) with focal plane on the GCL (A), on the IPL at 75% (B), 55% (C), and 35% (D) depths and on the INL (E). Arrowheads in panel A point to somata of homologously coupled ganglion cells, whereas arrows display cell bodies of heterologously coupled amacrine cells. Terminal dendrites of this G_{13} cell appear in all three focal planes of the IPL (B–D) indicating that dendrites of this G_{13} cell stratify diffusely. Arrowheads and arrows in E differentiate between small and large coupled amacrine cell somata, respectively. F: Camera-lucida drawing shows dendritic morphology of the same G_{13} cell. a, axon. Scale bar = 100 μm.

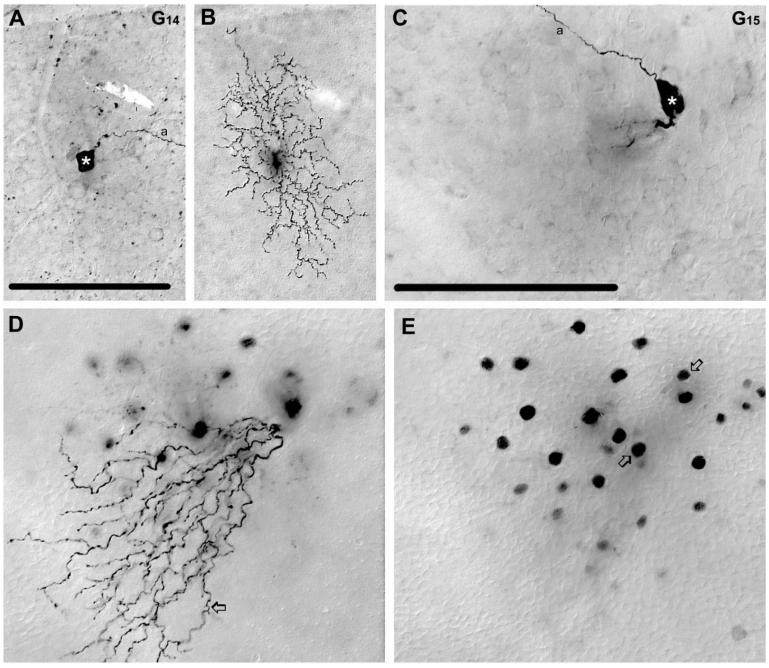

Figure 9.

Morphology and tracer coupling patterns of the G_{14} and G_{15} ganglion cell subtypes in the mouse retina. A,B: Pair of photomicrographs show a G_{14} cell (asterisk) with dendrites stratifying in the middle of the IPL. This G_{14} cell shows no evidence of tracer coupling. C–E: Photomicrographs show a G_{15} cell (asterisk) with focal depth on the GCL (C), on the IPL in (D), and on the INL (E). Arrow points to one of the wavy dendrites of this cell in panel D, whereas arrows point to somata of heterologously coupled amacrine cells in the INL in panel E. a, axon. Scale bars = 100 μm.

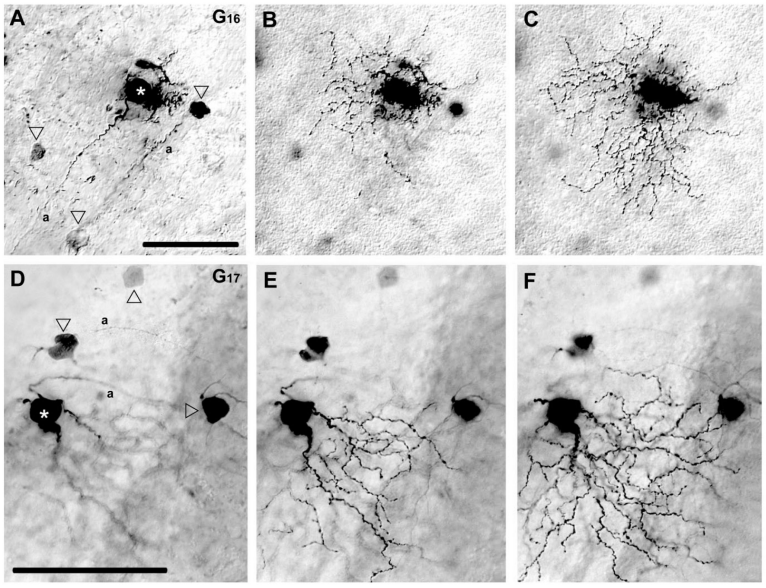

Figure 10.

Morphology and tracer coupling patterns of the G_{16} and G_{17} ganglion cells. A–C: Photomicrographs show a G_{16} cell (asterisk) with focal planes on the GCL (A), sublamina-b (B), and sublamina-a (C). This G_{16} cell shows homologous coupling to ganglion cells (arrowheads). Panels B and C show dendrites of the injected G_{16} cell stratifying either in sublamina-b or sublamina-a, respectively. D–F: Photomicrographs show a G_{17} cell (asterisk) at focal depths on the GCL (D), on sublamina-b of the IPL (E), and on sublamina-a of the IPL (F). Arrowheads in panel D point to cell bodies of homologously-coupled G_{17} cells. Panels E and F focus on dendrites of the injected G_{17} cell, which stratify either in sublamina-b or sublamina-a, respectively. a, axon. Scale bars = 50 μm in A–C; 50 μm in D–F.

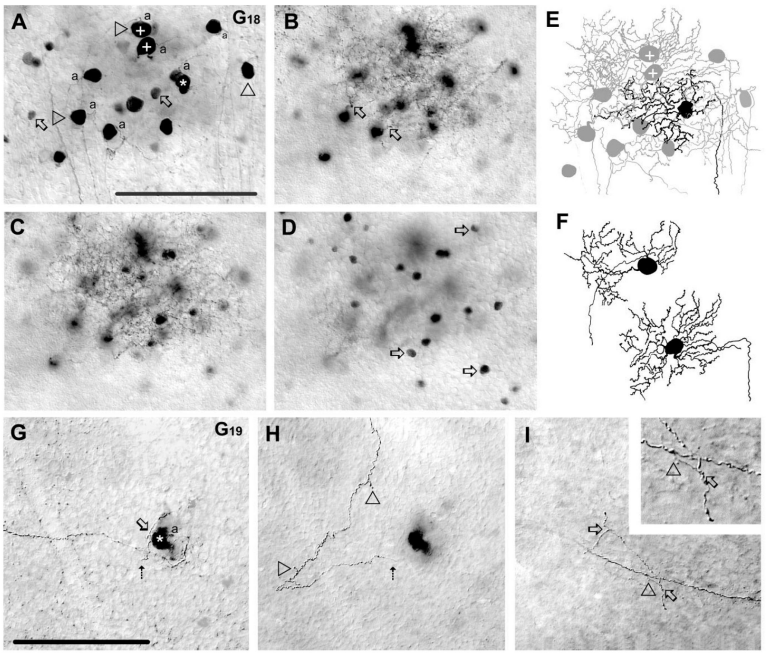

Figure 11.

Morphology and tracer coupling patterns of the G_{18} and G_{19} ganglion cell subtypes. A–D: Photomicrographs showing soma/dendritic morphology and coupling pattern of a G_{18} cell (asterisk). This G_{18} cell displays homologous coupling to an array of ganglion cell somata (arrowheads) and heterologous coupling to amacrine cells (arrows) in the GCL (A). The plus (+) signs mark the somata of the coupled ganglion cells drawn in panel F. Arrows in panel B point to emerging dendritic stalks of coupled ganglion cells in the proximal IPL, whereas panel C displays more distally located dendritic branches of labeled G_{18} cells. The labeled G_{18} cell also displays heterologous coupling to amacrine cells with somata that lay in the INL (arrows) (D). E: Camera-lucida drawing of the G_{18} ganglion cell shown in panels A–D showing the dendritic architecture of the injected (black) and coupled ganglion cells (gray); the plus signs mark coupled ganglion cells drawn in panel F. Note the extensive overlap of dendritic arbors of the injected and coupled G_{18} cells. F: Camera-lucida drawings of two coupled ganglion cells that share their soma/dendritic morphologies with the injected G_{18} cell. G–I: Photomicrographs showing a G_{19} cell (asterisk). The arrow points to the site where a dendrite emerges, whereas dotted arrow indicates where the dendrite leaves the plane of focus (G) and where it comes back into view in a more distal plane of the IPL (H). Arrowheads in panel H point to small dendritic side branches. Panel I shows the axon of this G_{19} cell, which shows clear sprouting (arrowhead), with daughter branches that enter the IPL and show two additional branch points (arrows). Inset enlarges the site of the primary (arrowhead) and one of the secondary (arrows) branch points. This G_{19} cell shows no evidence of tracer coupling. a, axon. Scale bars = 100 μm.

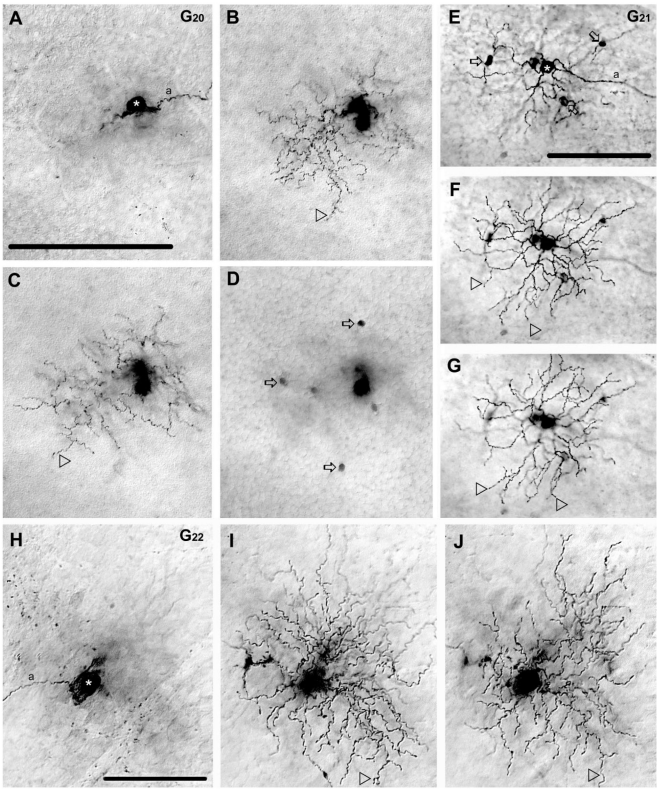

Figure 12.

Morphology and tracer coupling pattern of the G_{20},G_{21}, and G_{22} ganglion cell subtypes in the mouse retina. A–D: Photomicrographs show a G_{20} cell (asterisk) with focal depths on the GCL (A), on sublamina-b of the IPL (B), sublamina-a of the IPL (C), and in the INL (D). Arrowheads point to dendrites that stratify in either sublamina-b (B) or sublamina-a (C) of the IPL. Arrows in panel D point to somata of heterologously coupled amacrine cells in the INL. E–G: Photomicrographs show a G_{21} cell (asterisk) with focal depths on the GCL (E), on sublamina-b of the IPL (F), and sublamina-a (G) where dendrites stratify (arrowheads). This G_{21} cell displays tracer coupling to amacrine cells (arrows) with somata displaced into the GCL. H–J: Photomicrographs showing a G_{22} cell (asterisk) with focal depths on the GCL (H), sublamina-b (I), and sublamina-a (J) of the IPL. The dendritic arbor of this G_{22} cell appears bistratified with some terminal dendrites (arrowheads) located in sublamina-b (I) or sublamina-a (J). This G_{22} cell shows no evidence of tracer coupling. a, axon. Scale bars = 100 μm.

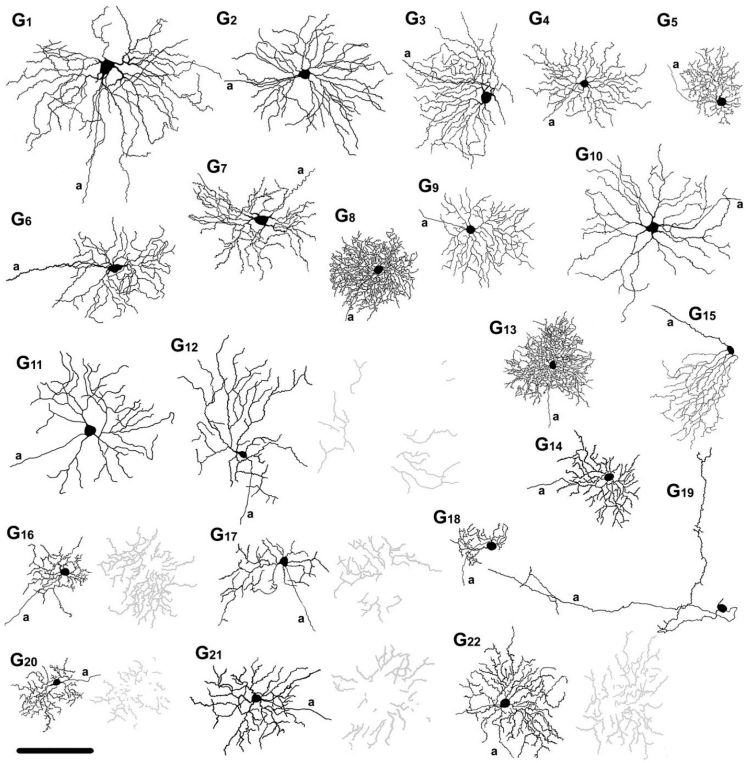

Figure 13.

Summary diagram showing camera lucida drawings of representative ganglion cells. G_1–G_{22} labels on the top represent the name of each ganglion cell subtype. Proximally and distally stratifying dendrites of bistratified ganglion cells are shown in black and gray, respectively. a, axon. Scale bar = 100 μm.

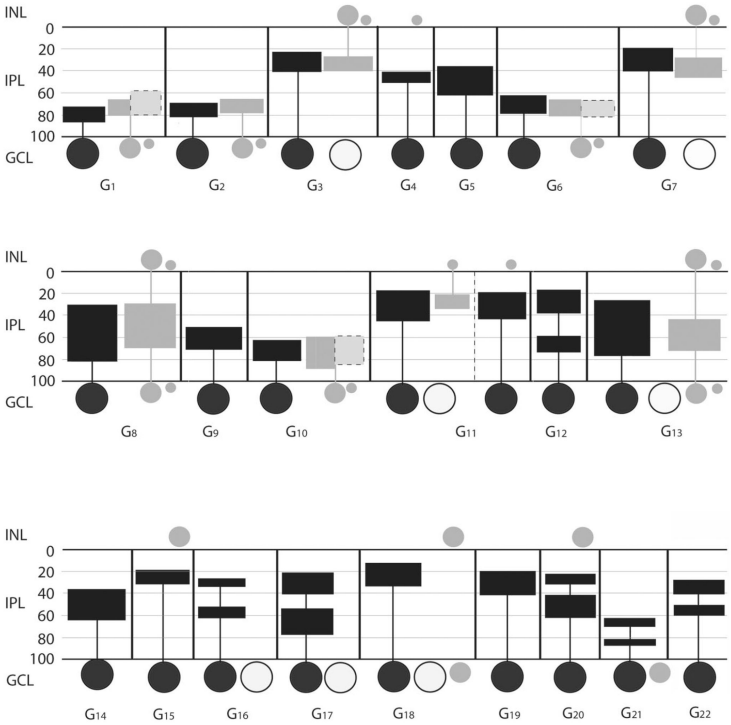

Figure 14.

Schematic summarizing the tracer coupling patterns of the 22 ganglion cell subtypes in the mouse retina. In addition to coupling, some morphological features of both injected and coupled cells are also shown, including dendritic and axonal (if any) stratification levels in the IPL, localization and relative soma sizes of both ganglion and amacrine cell somata. Black horizontal lines represent the scleral and vitreal borders of the IPL, whereas gray horizontal lines separate the five IPL strata. Numbers on the left represent percent depth levels in the IPL. Summary diagrams of ganglion cells are separated with vertical black lines for clear distinction between cell subtypes. Large filled circles represent the injected ganglion cell bodies in each box, whereas large open circles symbolize somata of tracer-coupled ganglion cells (if any). Gray filled circles represent somata of tracer-coupled amacrine cells. Sizes of gray spots reflect relative size differences among coupled amacrine cell somata. Filled rectangles connected to somata represent the maximum extent of dendritic arbors for injected ganglion cells (black), for amacrine cell dendrites (gray) and for amacrine cell axons (light gray with dashed frame). Note that the widths of rectangles do not reflect the diameter of the dendritic fields.

TABLE 1

Quantitative Data of Injected Ganglion Cells and Tracer Coupled Ganglion and Amacrine Cells (average ± SD)

Cell type	Soma size (μm)	DF diameter (μm)	Stratification level in IPL (%)	Coupling to GCs	Coupling to ACs in GCL	Coupling to ACs in INL
G1 (n=8)	20.3 ± 3.4	244.6 ± 29.9	78 ± 8.4	No	• 2–17 (m=8.7 ± 4.7) large AC; ss=10.4–13.4 μm; d.strat: 71.8% ± 8.6; a.strat: 69.3% ± 10.7; • 5–21 (m=12.75 ± 6.1) small AC; ss=7.1–8.6 μm.	No
G2 (n=19)	17.6 ± 2.9	200.3 ± 42.1	73.3 ± 8.1	No	• 2–7 (m=5.1 ± 2.8) large AC; ss=9–12 μm; d.strat: 71.7% ± 7.1; • 2–6 (m=4.3 ± 3.1) small AC; ss=6–9 μm.	No
G3 (n=58)	17.8 ± 2.3	185.4 ± 18.5	32.6 ± 9.1	3–8 (m=5.5 ± 2.5)	No	• 3–12 (m=6.21 ± 4.8 large AC; ss=8–11 μm; d.strat: 33.5% ± 7.; • 6–13 (mean = 8.1 ± 3.2 small AC; ss=6–8 μm
G4 (n=5)	12.7 ± 1.2	142.6 ± 25.1	45.7 ± 4.3	No	No	• 5–30 (m=18.5 ± 7.3 AC; ss=5–9 μm.
G5 (n=12)	11.4 ± 1	105.3 ± 23.6	50.1 ± 12.6	No	No	No
G6 (n=19)	19 ± 3	189 ± 30.1	69.9 ± 8.9	No	• 0–11 (m=4.5 ± 3.2 large AC; ss=10,6-12.2 μm; d.strat: 73.3% ± 7.8; a.strat: 74% ± 8.2; • 2–28 (m=12.2 ± 7.6 small AC; ss= 6–8.7 μm.	No
G7 (n=11)	19 ± 3.2	196.3 ± 18	30 ± 10.7	2–7 (m=3.9 ± 1.9)	No	• 0-5 (m=2.7 ± 1.8 large AC; ss=8.7-10.7 μm; d.strat: 37.1% ± 8.7); • 2–17 (m=7.2 ± 5 small AC; ss=4.9–6.5 μm.
G8 (n=8)	15.2 ± 1.8	164.9 ± 45.9	45 ± 13.2–67.7 ± 14.2	No	• 0–12 (m=5.3 ± 4.3 large AC; ss=9–11.4 μm; d.strat: 50.1% ± 17.6; • 0–19 (m=7.3 ± 6.9 small AC; ss=5.3–6.6 μm.	• 3–24 (m=7.7 ± 6.7 large AC; ss=8.8–9.2 μm; • 3–32 (m=9.9 ± 8.7 small AC; ss=4.4–5.7 μm.
G9 (n=8)	14.5 ± 1.8	165.6 ± 32.2	61.6 ± 9.5	No	No	No
G10 (n=8)	18.4 ± 2	247.5 ± 34.1	71.3 ± 9.6	No	• 7–12 (m=10 ± 2.6 large AC; ss=9–12.3 μm; d.strat: 69% ± 13.7; a.strat: 72.1% ± 12.4;	No

Cell type	Soma size (μm)	DF diameter (μm)	Stratification level in IPL (%)	Coupling to GCs	Coupling to ACs in GCL	Coupling to ACs in INL
					• 3–9 (m=5.8 ± 2.8 small AC; ss=6.6–7.4 μm.	
G11 (n=12)	16.9 ± 2.6	183.3 ± 30.5	31.4 ± 13.7	0–7 (m=3 ± 2.7)	No	• 2–36 (m=10.7 ± 10.8 small AC; ss=5.5–7μm.
G12 (n=3)	14.3 ± 2.5	201.2 ± 42.3	32.8 ± 11.7 and 66.7 ± 8.1	No	No	
G13 (n=9)	15.4 ± 2.9	159.8 ± 25.9	38.9 ± 13.7–65.4 ± 12.3	0–10 (m=4.4 ± 3.6)	• 0–7 (m=3.1 ± 2.5 large AC; ss=9.8–11.6 μm; d.strat: 59% ± 13.7;	• 4–22 (m=7.9 ± 5.7 large AC; ss=8.3–10 μm;
					• 2–6 (m=4.6 ± 1.7 small AC; ss=5–6.8 μm.	• 1–22 (m=10.9 ± 7.6 small AC; ss=4.7–6 μm.
G14 (n=3)	13 ± 1.8	135 ± 23.8	51.2 ± 13.6	No	No	No
G15 (n=3)	18 ± 2.5	153 ± 27	24.6 ±6	No	No	• 9–31 (m=20 ± 11 AC; ss=5.7–7.7 μm;
G16 (n=3)	13.9 ± 3.7	123 ± 18.7	30 ± 3.8 and 56 ± 5.9	2–3 (m=2.5 ± 0.7	No	No
G17 (n=16)	15.3 ± 1.6	159.3 ± 8.5	31.9 ± 11.2 and 67.8 ± 10.3	1–17 (m=5.8 ± 4.3)	No	No
G18 (n=1)	15	62.5	25.2 ± 9.7	11	10 (ss=6.4–8 μm)	22 (ss=6.2–8.1 μm)
G19 (n=1)	11	NA	28.9 ± 11.4	No	No	No
G20 (n=1)	14	117	27.6 ± 4.8 and 51.4 ± 9.7	No	No	6 (ss=5–6 μm)
G21 (n=1)	15	162	66.5. ± 2.7 and 83.7 ± 2.7	No	5 (ss=5–6 μm)	No
G22 (n=1)	17	122	36.7 ± 8.3 and 56.7 ± 3.3	No	No	No

DF, dendritic field; IPL, inner plexiform layer; GCs, ganglion cells; GCL, ganglion cells layer; ACs, amacrine cells; INL, inner nuclear layer; m, mean; ss, soma size (largest diameter); d.strat, dendritic stratification; a.strat, axonal stratification.

TABLE 2

This Table Lists the Ganglion Cell Populations Described in This Study and Previously Described Mouse Ganglion Cells that Display Equivalent Morphologies

GC type	Sun et al., 2002	Badea and Nathans, 2004	Kong et al., 2005	Coombs et al., 2006	Other mouse GCequivalents	Equivalents of tracer-coupled ACs
G_1	A1	Mon. cluster 9	Cluster 11	M10		- WA4-1 (Lin and Masland, 2006) - PA-S5 (Perez De Sevilla Muller et al., 2007)
G_2	$A2_i$	Mon. cluster 9	Cluster 8	M8, M9(on)	- ON alpha GCs (Schubert et al. 2005a) - ON alpha GCs (Völgyi et al. 2005)	- giant GC (Badea and Nathans, 2004)
G_3	$A2_o$	Mon. cluster 7	Cluster 10	M9(off)	- OFF alpha GCs (Schubert et al. 2005a) - OFF alpha GCs (Völgyi et al. 2005)	- widefield cluster 3 (Badea and Nathans, 2004) - WA2-2 (Lin and Masland, 2006)
G_4	B1	Mon. cluster 1	Cluster 2	M3(off)		
G_5	B2	Mon. cluster 2, 4	Cluster 1	M11		
G_6	$B3_i$	Mon. cluster 9	Cluster 4	M7(on), M3(on)		- WA4-1 (Lin and Masland, 2006) - PA-S5 (Perez De Sevilla Muller et al., 2007)
G_7	$B3_o$	Mon. cluster 7	Cluster 6	M6(off)		- wide-field cluster 3 (Badea and Nathans, 2004) - WA2-2 (Lin and Masland, 2006)
G_8	B4	Mon. cluster 2, 4	Cluster 1	M1, M11		- WA3-2 (Lin and Masland, 2006)
G_9	C1	Mon. cluster 1	Cluster 2, 7			
G_{10}	$C2_i$	Mon. cluster 9	Cluster 11	M6(on), M10		- WA4-1 (Lin and Masland, 2006)
G_{11}	$C2_o$	Mon. cluster 7		M6(off)		
G_{12}	C3			M6(on), unnamed bistratified cell	- type 1 GC (Schubert et al., 2005b)	
G_{13}	C4	Mon. cluster 4, 5	Cluster 1	M11		
G_{14}	C5	Mon. cluster 1-2	Cluster 2	M3(off)		
G_{15}	C6	Mon. cluster 6		M5a	- JAM-B-positive cells (Kim et al., 2008)	
G_{16}	D1	Bi. cluster 1			- type 3 GC (Schubert et al., 2005b)	
G_{17}	D2	Bi. cluster 2, 3		M12, M13, M14	- type 2 GC (Schubert et al., 2005b)	
G_{18}		Mon. cluster 4	Cluster 6			
G_{19}						
G_{20}		Mon. cluster 4		M13		

GC type	Sun et al., 2002	Badea and Nathans, 2004	Kong et al., 2005	Coombs et al., 2006	Other mouse GCequivalents	Equivalents of tracer-coupled ACs
G_{21}		Mon. cluster 5		M13		
G_{22}		Bistrat. Cluster 1,2		M12,13,14		

Last column shows previously described amacrine cell equivalents of coupled amacrine cells in this study that appear in coupled arrays of the appropriate ganglion cell injections (same row).